Estimation of Nitrogen Content of Rice Plants and Protein Content of Brown Rice Using Ground-Based Hyperspectral Imagery

HIROYUKI ONOYAMA

2016

Laboratory of Field Robotics

Division of Environmental Science and Technology

Graduate School of Agriculture

Kyoto University

Abstract

In this dissertation, the estimation of nitrogen content of rice plants and protein content of brown rice using ground-based hyperspectral imagery are investigated. To provide an overview of this research, a brief summary is given below.

Currently, rice is a staple food for more than 3 billion people in the world. Moreover, the world population is projected to grow to 7 to 9 billion by 2050 with demand for rice outstripping supply. However, inefficient agricultural activity, such as excessive nitrogen application for productivity gains, has and will continue to lead to degradation of the environment if nothing is done about it. Moreover, farmers are interested in maximizing yields and profits, while consumers are increasingly demanding high quality agricultural products. Meeting these sophisticated and diversified needs will demand more from agriculturalists than ever before. This is where the concept of precision agriculture has emerged to meet these sophisticated and diversified needs.

Management of crop variability is one component of precision agriculture. While minimizing crop spatial and temporal variability, it is also possible to optimize simultaneously both profitability and environmental conservation. For example, rice plant variability in crop traits that arise during growth can lead to quantitative and qualitative differences in harvested rice. Thus, it is important to develop techniques to visualize these preharvest crop traits so as to be able better control their variability to meet the above mentioned multiple demands. In the case of the rice crop, nitrogen content of rice plants at both panicle initiation and heading stage, and protein content just before harvest are key factors to control the variability of yield and quality (taste). Therefore, measurements of these factors using remote sensing with high resolution (1 × 1 mm) hyperspectral imaging were applied.

Nitrogen content (g/m^2) of rice plants is the product of dry mass per unit area and nitrogen concentration. It is difficult to explain all the variance of the nitrogen content using the spectral features of rice plants because they relate to concentration. For instance, variation in plant growth rates can result from temperature differences. Thus, a partial least squares regression (PLSR) model that incorporates both the reflectance and growing degree-days (GDD) was constructed and evaluated. The results demonstrate that such an approach is adaptable enough to account for variations in inter-annual growing conditions for the prediction of rice nitrogen content at both the

panicle initiation and heading stage.

In order to improve the accuracy of rice protein content, estimation models were generated from the mean reflectance of five regions of interest (ROIs): the overall target area, non-canopy area (stems and soil), canopy area (leaves, yellow leaves, and ears), leaf area, and ear and yellow leaf area. These were compared to identify which part is most suitable for estimation in terms of accuracy. The results obtained show all models estimated rice protein content with high accuracy; no significant differences in estimation errors between the models was found with an analysis of variance (ANOVA). As a result, to minimize processing time, no segmentation of the image is recommended.

These results provide a method for estimating the nitrogen content of rice plants more precisely and refining the required specifications for remote sensing. As a consequence, these finer scaled more accurate determinations of crop nitrogen variation can be expected to improve crop management decisions, reduce input costs and environmental degradation associated with fertilizers, and inform more homogenous harvesting of crop traits such as taste, as well as determine the altitude needed for remote sensing platforms when imaging rice fields just before harvest.

Acknowledgements

I would like to first express my special gratitude to supervisor Dr. Michihisa IIDA, Professor of Laboratory of Field Robotics, Kyoto University, for his guidance and support during the duration of my Bachelor's, Master's and Doctor's program. If it had not been for his thoughtful guidance, advice and encouragement, this dissertation could have never been completed.

I would also like to gratefully and sincerely express my gratitude to the dissertation committee, Dr. Naoshi KONDO, Professor of Kyoto University and Dr. Kimihito NAKAMURA, Associate Professor of Kyoto University, for their suggestive and helpful comments with profound and comprehensive scholarly knowledge, and deep insight into the science.

I would like to express my sincere thankful to Dr. Masahiko SUGURI, Assistant Professor of Kyoto University, Dr. Katsuaki OHDOI, Assistant Professor of Kyoto University, Mr. Ryohei MASUDA, Assistant Professor of Kyoto University, and Dr. Chanseok RYU, Assistant Professor of Geyongsang National University, Korea, for their useful and appropriate advice. Dr. Masahiko SUGURI and Dr. Chanseok RYU especially provided support during the field experiments. Dr. Katsuaki OHDOI, who is the chief of the Bioproduction Engineering Research Facility, eagerly guided me on how to use the facility.

I would also like to express my sincere thankful to Dr. Tatsuya INAMURA, Professor of Kyoto University, Dr. Hiromo INOUE, Associate Professor of Kyoto University, Dr. Hiroshi SHIMIZU, Professor of Kyoto University, Dr. Hiroshi NAKASHIMA, Associate Professor of Kyoto University, Dr. Yuichi OGAWA, Associate Professor of Kyoto University, Dr. Juro MIYASAKA, Assistant Professor of Kyoto University, and Mr. Tetsuhito SUZUKI, Assistant Professor of Kyoto University, for their helpful advice.

I would like to deeply show my thanks to Dr. Garry PILLER, Associate Professor of Kyoto University. He kindly spared his precious time and effort to proofread my manuscript and managed to polish the English expressions.

Sincere thanks are also extended to all of the members in Laboratory of Field Robotics, Kyoto University. Ms. Masami KUBO, the secretary of the laboratory, supported my academic life with warmth. Dr. Hiroki KURITA always encouraged me with his undying friendship and his faithful attitude toward research. Dr. Wonjae CHO helped me with his knowledge about image processing and various hardware goods. I wish to express my gratitude to the members of the Remote Sensing Team; Teppei KURIMOTO, Ryo SASAKI, Jun NAKADE, Yusuke SOHARA, Shun ISHIKAWA, Takuma NISHIKAWA, Masataka YAGAWA, Yuta KATAOKA, and Keigo ITO, for their help with the experiments.

I wish to thank Nakanishi Shougakukai, Showa Houkoukai and Japan Society for the Promotion Science (JSPS), for financial assistance.

Finally, I wish to express my thanks and appreciation to my dear parents: Keiichi ONOYAMA and Yukiko ONOYAMA. I also wish to express my thanks to other family members; my big sister, Masako; my big brother, Takaya; my nieces, Ayane, Shion and Sara; my nephews, Keito and Yusei. Thanks to them, I was able to have a very fulfilling life until now and from now on.

Abbreviations

PLSR	Partial Least Squares Regression
NIR	Near-InfraRed
GDD	Growing Degree-Days
ROI	Region Of Interest
ENVI	ENvironment for Visualizing Images software
NDVI	Normalized Difference Vegetation Index
GNDVI	Green Normalized Difference Vegetation Index
R^2	coefficient of determination
RMSE	Root Mean Squares Error
RE	Relative Error
LVs	Latent Variables
GIS	Geographic Information System
UAV	Unmanned Aerial Vehicle
ANOVA	ANalysis Of Variance

Contents

List of Tables

List of Figures

Estimation of Nitrogen Content of Rice Plants and Protein Content of Brown Rice Using Ground-Based Hyperspectral Imagery

Chapter I Introduction

1.1 Background

Rice is a staple food for more than 3 billion people in the world (IRRI, 2010). Based on world population projections, the population will grow to 7 billion to 9 billion by 2050 (Fig. 1.1) and demand for rice will outstrip supply (UN DESA, 2013). However, increasing the amount of arable land is limited (Fig. 1.1) and inappropriate agricultural activity such as excessive nitrogen application in order to improve productivity leads to degradation of the environment. Moreover, farmers are interested in obtaining high yields and increased profits, while consumers demand high quality agricultural products. Therefore, agriculture needs to meet sophisticated and diversified needs more than ever before. The concept of precision agriculture has emerged to meet these sophisticated and diversified needs. Similarly, in Japan, rice is a staple food and the above mentioned multiple demands are present. Describing the circumstances for initiating precision agriculture here is important.

The Japanese government has been pressing ahead with fundamental domestic reforms in the agricultural sector for the liberalization of trade. However, the Japanese agricultural sector has had many problems; aging of the work force, shortage of successors, and low profitability. Thus, if Japanese agriculture was exposed to fierce global competition without taking any countermeasures, it could not be sustainable. To ensure food security, sustainability of agriculture would be required. One of the fundamental domestic reforms is aggregation of farmland and large-scale farming.

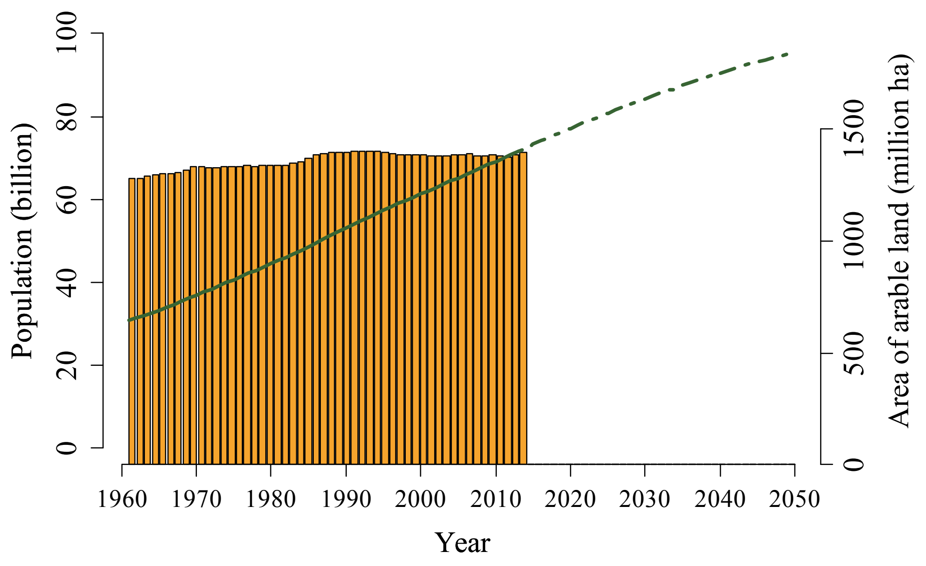

Fig. 1.1 World population prospect and area of arable land

Aggregation of farmland and large-scale farming bring about working efficiency and profitability, however, it has the disadvantage of increasing agricultural work while risking poor control of delicate cropping operations such as fertilizer application. Thus, it is necessary to develop automated agricultural machinery and to introduce management technology of crops, namely precision agriculture. This machinery and technology would enable farmers to compensate for the shortage of work force and simplify the entry of people engaging in farming. The automated agricultural machine for a tractor (Kise et al., 2001; Takai et al., 2010), a rice transplanter (Nagasaka et al., 2004; Nagasaka et al., 2009), and a head-feeding combine (Sato et al., 1996; Kurita et al., 2012; Iida et al., 2013; Iida et al., 2013; Saito et al., 2012; Kurita et al., 2014) have been developed.

Management of crop variability is one component of precision agriculture. While minimizing crop spatial and temporal variability it is also possible to pursue profitability and environmental conservation at the same time. In rice plants variability in crop traits during growth can lead to quantitative and qualitative differences in harvested rice. Thus, it is important to develop techniques to visualize these preharvest crop traits so as to be able control their variability to meet the above mentioned multiple demands.

Nitrogen, which is an essential plant nutrient, is a key factor in the control of variability in the quantity and quality of rice. Figure 1.2 shows a rice cultivation calendar. The panicle initiation stage, the heading stage and harvesting time are about 55, 80 and 120 days after transplanting, respectively.

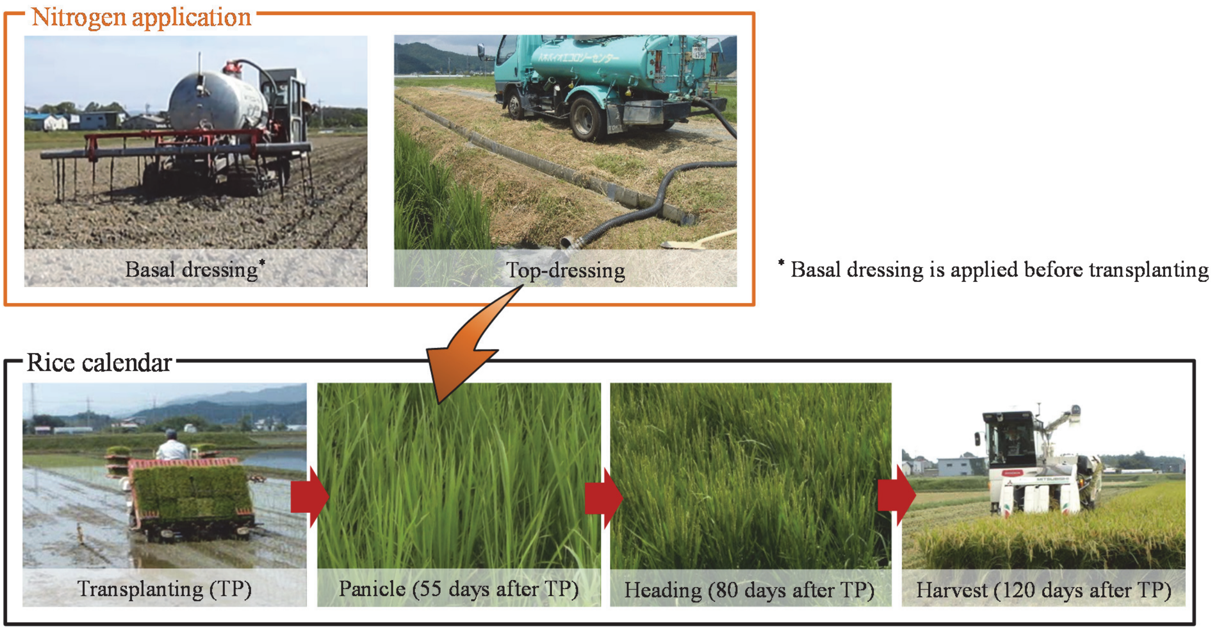

Fig. 1.2 Rice cultivation calendar

Normally in Japan, nitrogen is applied as a basal dressing before transplanting and a top-dressing is applied at the panicle initiation stage. Rice plant nitrogen estimation at the panicle initiation stage is important. This is because the protein content of rice prior to harvest ($P_{harvest}$), which is related to taste quality, and yield is predictable by the relationship between the rice plant nitrogen content at the panicle initiation stage ($N_{panicle}$) and the amount of top-dressing (Ryu et al., 2009; Ozaki et al., 2012). Miyama and Okabe (1984) reported the optimum amount of nitrogen content at heading stage. Thus, if the nitrogen content of rice plants at heading stage ($N_{heading}$) can be estimated, assessing the fertilizer response of top-dressing in each field will be possible and the result of this assessment can be used for next year's basal dressing fertilizer application. $P_{harvest}$ can be estimated, taste dependent harvesting and storage of rice will be possible. Therefore, measurements of $N_{panicle}$, $N_{heading}$ and $P_{harvest}$ are needed in order to improve rice production, both in terms of yield and quality. Figure 1.3 shows an example of precision agriculture for rice cropping.

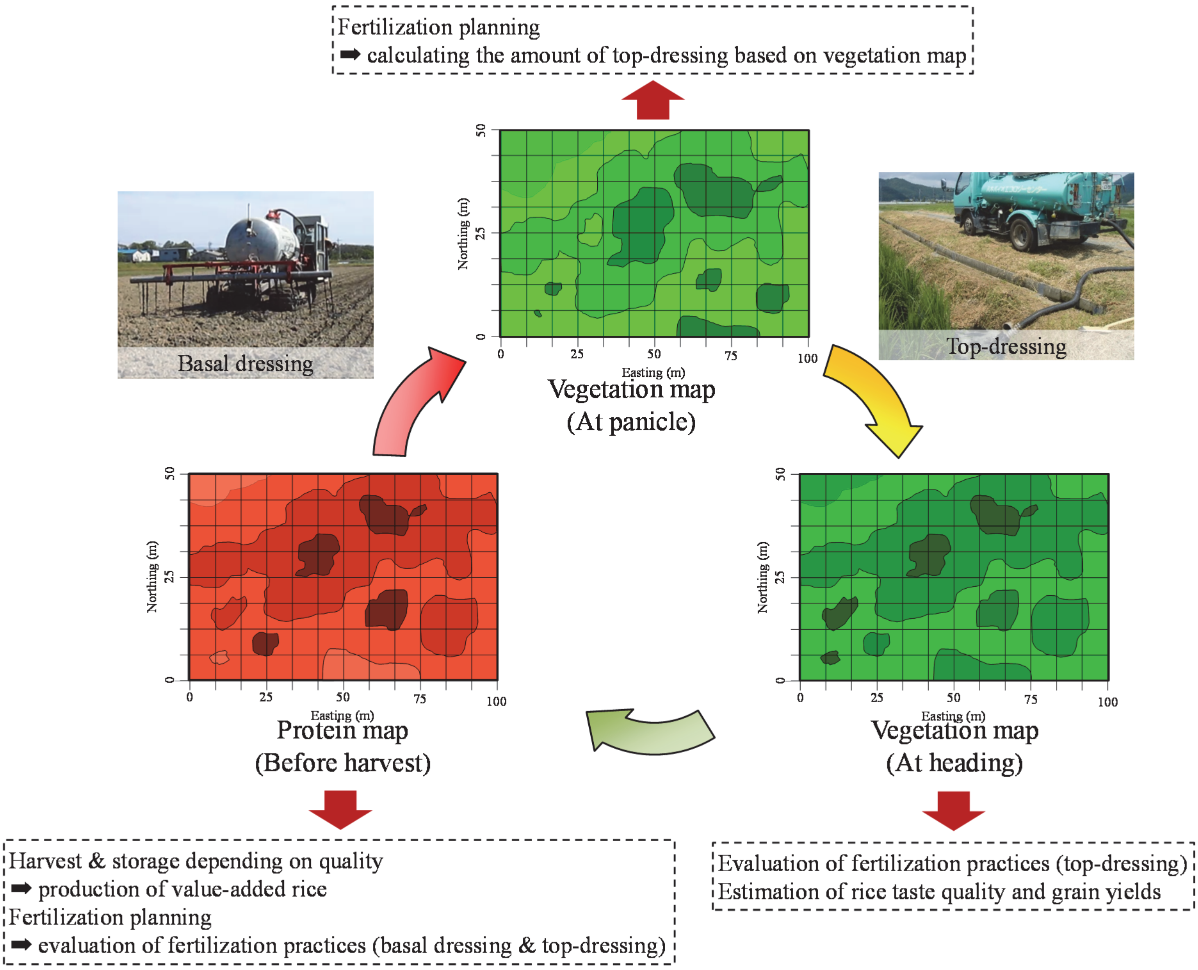

Fig. 1.3 Precision agriculture for rice cropping

Visualization techniques based on remote sensing have shown the capability of non-destructively estimating crop biochemical or physiological properties from crop canopy reflectance. Figure 1.4 shows a sample image of visualizing variability using aerial remote sensing. As can be seen from the figure, the variability of the vegetation is clear. There are a wide range of combinations of sensors and platforms that can be used for remote sensing. Remote sensing platforms such as satellite-based, aerial-based, and ground-based, have proven to be potential sources of collecting various spectral features of vegetation. Multispectral camera, hyperspectral spectroradiometer or camera are widely used as sensors for visualizing agricultural crop traits. In this thesis, ground-based hyperspectral imaging was applied.

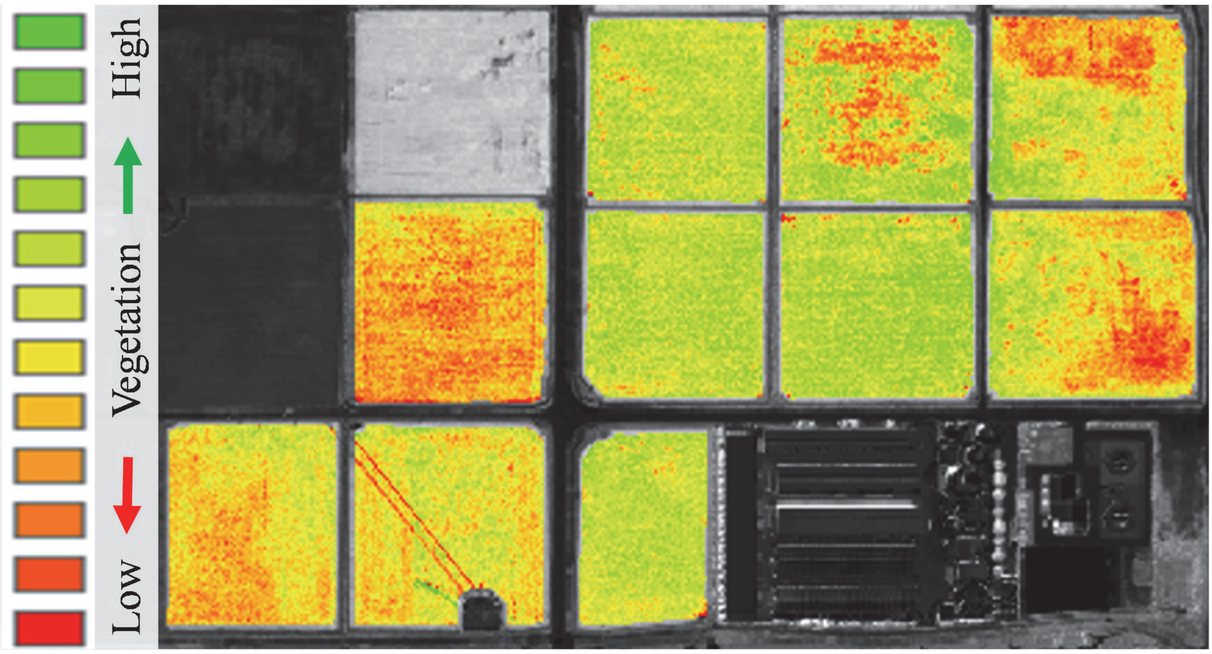

Fig. 1.4 Visualizing the variability of vegetation

The spatial resolution of ground-based remote sensing is high and prediction capabilities may be improved, although the area of application is smaller than that of satellite-based or aerial-based methods. Compared to the multispectral sensor, the hyperspectral sensor can obtain continuous spectrum, and is sensitive to the changes in narrow absorption features, and thus can detect crop biochemical properties more precisely. In ground-based remote sensing, spectrometers have been widely used, but the data obtained is one-dimensional. Consequently, the data includes the reflectance not only of the desired target but also of non-targets (White et al., 2000), such as soil background and ponding water in the case of rice paddies. A hyperspectral image, in contrast, provides a three-dimensional spatial and spectral data cube from which you can extract the reflectance of only the target. Figure 1.5 shows a high resolution two-dimensional NIR image. When appropriate image processing is applied to the image, the accuracy of an estimation model can be enhanced.

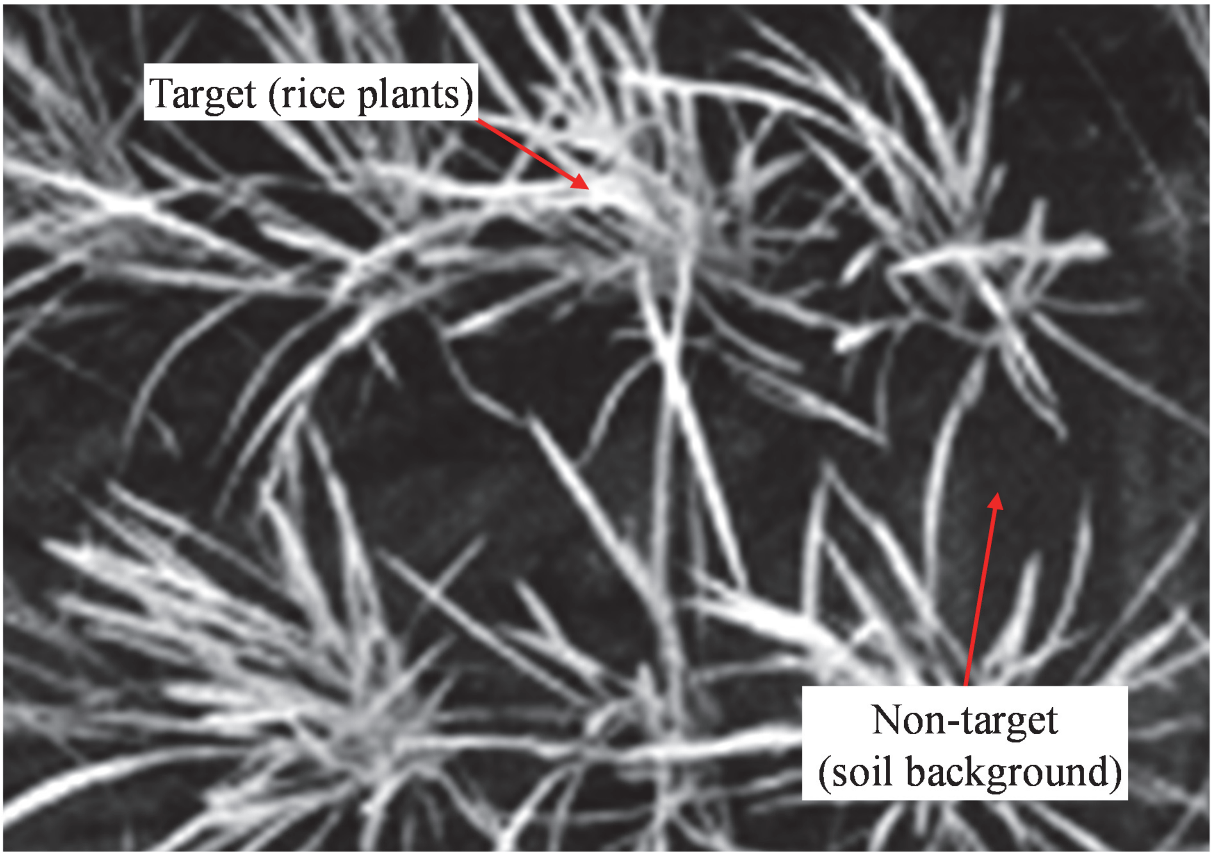

Fig. 1.5 High resolution two-dimensional NIR image

Recently, hyperspectral imaging systems have been studied. The potential of hyperspectral imaging for the classification and characterization of turkey hams was investigated (ElMasry et al., 2011). It is also possible to detect various common defects on an orange surface (Li et al., 2011). Hyperspectral imaging system was effective for the nondestructive measurement of localized nitrate concentration in a leaf of *komatsuna* (*Brassica rapa* var. *peruviridis*) (Itoh et al., 2010). In addition to these laboratory-based studies, a system to map the herbage mass of perennial ryegrass using field-based hyperspectral imaging has been reported (Suzuki et al., 2012).

Partial least squares regression (PLSR) modeling has desirable properties that improve the precision of the modeling parameters with an increasing number of relevant variables and observations (Wold et al., 2001). PLSR analysis is one of the most efficient methods for extracting and creating reliable models in a wide range of fields (Nguyen and Lee, 2006) and when applied to hyperspectral reflectance data, it may be useful as an exploratory and predictive tool (Hansen and Schjoerring, 2003).

It can be difficult to estimate the nitrogen content of rice plants at the panicle initiation stage and at heading stage using remote sensing techniques. Because leaf color obtained by remote sensing relates to not the amount of nitrogen but to the concentration of nitrogen. From a practical standpoint, a prediction model should have the ability to estimate crop status from new remote-sensing data with a desired precision or accuracy. For the purpose of developing a model that considers growing condition, a mutual prediction was calculated by use of a single year's data for the training set and the remaining years' data for the test set (Ryu et al., 2011). Remote sensing models may be affected by differences in environmental variables, such as weather conditions (Ryu et al., 2009, 2011). Although growing temperature mainly constrains the developmental rate, it also indirectly influences the amount of growth; the sooner the tillering stage begins due to relatively high growing temperature, the higher the increase in the number of leaves on the main axis (the amount of growth). In the results of mutual estimation, the amount of growth owing to the effect of growing temperature is over- or underestimated by ground-based hyperspectral imaging. The influence of growing temperature on growth rate might be quantified to improve the accuracy of the mutual estimation. Thus, to estimate the amount of rice plants nitrogen per unit area at the panicle initiation stage and heading stage, I proposed the construction method of the hyperspectral imaging model that integrates growing temperature data.

The canopy structure of rice plants before harvest is composed of ears and leaves. Ishii and Katano (2008) estimated the rice protein content from the leaf blade's SPAD-502 chlorophyll meter (Konica Minolta, Inc., Tokyo, Japan) value. Onoyama et al. (2011) estimated it from the reflectance of rough rice. Ryu et al. (2011a) estimated it from the whole canopy reflectance of the rice plant. However, the exact part of the rice plant that is suitable for the estimation of the rice protein content has not yet been identified. Thus, I apply region of interest (ROI) analysis, which segments the image into categories such as the leaf, ear, or whole rice plant, extract the spectral information of each segment, and then compare the model accuracies derived from each ROI reflectance. From this information, the appropriate preprocessing can be proposed for the estimation of protein content of rice plants just before harvest.

In this thesis, ground-based hyperspectral remote sensing was applied. Its spatial resolution is high, although the area of application is smaller than that of satellite-based or aerial methods.

Moreover, hyperspectral imaging provides a three-dimensional spatial and spectral data cube that enables the extraction of reflectance from only the target, thus, the potential is there to increase prediction capabilities. If field data for rice, such as basal dressing, topdressing, temperature data and remote sensing data, are input into a geographic information system (GIS), then management and improvement of rice taste quality and yield may be possible.

1.2 Objectives and Overview

This research aims to estimate important rice crop traits at critical points during its growth using ground-based hyperspectral imagery in order to aid better precision agriculture management decisions. The objectives of this thesis are as follows:

1. To estimate the nitrogen content of rice plants at panicle initiation stage
2. To estimate the nitrogen content of rice plants at heading stage
3. To estimate the protein content of rice grain just prior to harvest

The contents of each chapter are briefly described below.

This thesis reports three years' field studies. Field experiments, hyperspectral imaging system and analysis procedures are introduced in Chapter II. In Chapter III, I demonstrate the effectiveness of a PLSR model that incorporates both the reflectance and growing degree-days (GDD) at panicle initiation stage. Similarly, I demonstrate the effectiveness of a PLSR model that incorporates both the reflectance and GDD at heading stage in Chapter IV. In Chapter V, I compare the accuracy of rice protein content estimation of various models generated from the mean reflectances of five regions of interest (ROIs). Finally, the conclusions of the thesis are outlined in Chapter VI.

References

ElMasry, G., A. Iqbal, D.-W. Sun, P. Allen, and P. Ward. 2011. Quality classification of cooked, sliced turkey hams using NIR hyperspectral imaging system. *Journal of Food Engineering* 103(3):333-344.

Hansen, P., and J. Schjoerring. 2003. Reflectance measurement of canopy biomass and nitrogen status in wheat crops using normalized difference vegetation indices and partial least squares regression. *Remote sensing of Environment* 86(4):542-553.

Iida, M., H. Kurita, W.-J. Cho, Y. Mochizuki, R. Yamamoto, M. Suguri, and R. Masuda. 2013a. Turning Performance of Combine Robot by Various Compasses. In *Agricontrol*.

Iida, M., R. Uchida, H. Zhu, M. Suguri, H. Kurita, and R. Masuda. 2013b. Path-following control of a head-feeding combine robot. *Engineering in Agriculture, Environment and Food* 6(2):61-67.

IRRI. 2010. Sustainable crop productivity increase for global food security I. R. R. Institute, ed.

Ishii, K., and M. Katano. 2008. Growth diagnosis of yield and protein content of brewery's rice "Yamada-nishiki" by the SPAD value of leaf blade. *Report of the Kyushu Branch, Crop Science Society of Japan*(74):27-30.

Itoh, H., S. Kanda, H. Matsuura, N. Shiraishi, K. Sakai, and A. Sasao. 2010. Measurement of nitrate concentration distribution in vegetables by near-Infrared hyperspectral imaging. *Environment control in biology* 48(2):37-49.

Kise, M., N. Noguchi, K. Ishii, and H. Terao. 2001a. Field mobile robot navigated by RTK-GPS and FOG (Part 1). *Journal of the Japanese Society of Agricultural Machinery* 63(5):74-79.

Kise, M., N. Noguchi, K. Ishii, and H. Terao. 2001b. Field mobile robot navigated by RTK-GPS and FOG (part 2). *Journal of the Japanese Society of Agricultural Machinery* 63(5):80-85.

Kise, M., N. Noguchi, K. Ishii, and H. Terao. 2002a. Field mobile robot navigated by RTK-GPS and FOG (Part 3). *Journal of the Japanese Society of Agricultural Machinery* 64(2):102-110.

Kise, M., N. Noguchi, K. Ishii, and H. Terao. 2002b. Field mobile robot navigated by RTK-GPS and FOG (Part 4). *Journal of the Japanese Society of Agricultural Machinery* 64(4):76-84.

Kurita, H., M. Iida, M. Suguri, and R. Masuda. 2012. Application of Image Processing Technology for Unloading Automation of Robotic Head-Feeding Combine Harvester. *Engineering in Agriculture, Environment and Food* 5(4):146-151.

Kurita, H., M. Iida, M. Suguri, R. Masuda, and W. Cho. 2014. Efficient searching for grain storage container by combine robot. *Engineering in Agriculture, Environment and Food* 7(3):109-114.

Li, J., X. Rao, and Y. Ying. 2011. Detection of common defects on oranges using hyperspectral reflectance imaging. *Computers and electronics in Agriculture* 78(1):38-48.

Miyama, M., and T. Okabe. 1984. A suitable nitrogen fertilization method for several crop plants based on optimum nitrogen content, 1: Differences in optimum nitrogen content among rice varieties. *Journal of the science of soil and manure* 55(1):1-8.

Nagasaka, Y., H. Saito, K. Tamaki, M. Seki, K. Kobayashi, and K. Taniwaki. 2009. An autonomous rice transplanter guided by global positioning system and inertial measurement unit. *Journal of Field Robotics* 26(6–7):537-548.

Nguyen, H. T., and B.-W. Lee. 2006. Assessment of rice leaf growth and nitrogen status by hyperspectral canopy reflectance and partial least square regression. *European Journal of Agronomy* 24(4):349-356.

Onoyama, H., C. Ryu, M. Suguri, and M. Iida. 2011. Estimation of Rice Protein Content Using Ground-Based Hyperspectral Remote Sensing. *Engineering in Agriculture, Environment and Food* 4(3):71-76.

Ozaki, K., T. Kobayashi, Y. Ohashi, and K. Kawase. 2012. Establishment of Predict Method to Regulate Desirable Spikelet Numbers and Protein Contents by Growth Diagnosis Production, and Application to 'Koshihikari' Cultivated in Tango Area, Kyoto Prefecture. *Bulletin Of The Agricultural And Forestry Technology Department, Kyoto Prefectural Agriculture, Forestry And Fisheries Technology Center 'Agriculture Section'* 35:1-10.

Ryu, C., M. Suguri, M. Iida, M. Umeda, and C. Lee. 2011a. Integrating remote sensing and GIS for prediction of rice protein contents. *Precision Agriculture* 12(3):378-394.

Ryu, C., M. Suguri, and M. Umeda. 2009. Model for predicting the nitrogen content of rice at panicle initiation stage using data from airborne hyperspectral remote sensing. *Biosystems engineering* 104(4):465-475.

Ryu, C., M. Suguri, and M. Umeda. 2011b. Multivariate analysis of nitrogen content for rice at the heading stage using reflectance of airborne hyperspectral remote sensing. *Field Crops Research* 122(3):214-224.

Saito, M., K. Tamaki, K. Nishiwaki, and Y. Nagasaka. 2012. Development of an autonomous rice combine harvester using CAN bus system. *Journal of the Japanese Society of Agricultural Machinery* 74(4):312-317.

Sato, J., K. Shigeta, and Y. Nagasaka. 1996. Automatic operation of a combined harvester in a rice field. In *Multisensor Fusion and Integration for Intelligent Systems, 1996. IEEE/SICE/RSJ International Conference on*. IEEE.

Suzuki, Y., H. Okamoto, M. Takahashi, T. Kataoka, and Y. Shibata. 2012. Mapping the spatial distribution of botanical composition and herbage mass in pastures using hyperspectral imaging. *Grassland science* 58(1):1-7.

Takai, R., O. Barawid, K. Ishii, and N. Noguchi. 2010. Development of crawler-type robot tractor based on GPS and IMU. In *Agricontrol*.

Uchida, R., M. Iida, H. Zhu, H. Kurita, M. Suguri, and R. Masuda. 2013. Path Following Control for Head-feeding Combine Robot. *Transactions of the Society of Instrument and Control Engineers* 49(1):119-124.

UN DESA. 2013. World Population Prospects: The 2012 Revision. United Nations, Department of Economic and Social Affairs, Population Division New York, NY, USA.

White, J., C. Trotter, L. Brown, and N. Scott. 2000. Nitrogen concentration in New Zealand vegetation foliage derived from laboratory and field spectrometry. *International Journal of Remote Sensing* 21(12):2525-2531.

Yoshisada, N., U. Naonobu, and K. Yutaka. 2004. Automated rice transplanter using global positioning and gyroscopes. *Computers and electronics in Agriculture* 43(3):223-234.

Chapter II

Field Experiments, Equipment and Statistical Procedures

2.1 Field Experiments

The field experiments took place in Yagi Town, Nantan City, Kyoto Prefecture, Japan (135°55′E, 35°09′N; 125 m above sea level) (Fig. 2.1). Four fields were observed over three years (2008–2010). The area of each field was approximately 0.25 ha and the soil type was silty clay. The tested rice was *Oryza sativa L*. and the variety was *Kinu-Hikari*. The interrow and intrarow spacing of rice were planted in approximately 30 cm and 16 cm, respectively. For each field there were 8–10 sampling points (Fig. 2.2), resulting in 34, 33, 32 total sampling points in each of the respective years. Nitrogen fertilizer was applied as a basal dressing 1–3 weeks before rice transplanting and as a top-dressing at panicle initiation stage (Table 2.1). In this study, methane fermentation digested sludge was used as nitrogen fertilizer. The nitrogen conditions in the experimental field were modeled based on the standard amount in the district. Daily average temperature data were obtained from the Japan Meteorological Agency. To construct the model that incorporates differences in growing degree-days (GDD) between years, GDD was calculated as shown in equation (2.1) (McMaster and Wilhelm, 1997).

$$\mathrm{GDD} = \left(\frac{T_{MAX} + T_{MIN}}{2} \right) - T_{BASE} \tag{2.1}$$

where T_{MAX} and T_{MIN} are the daily maximum and minimum air temperature, respectively, and T_{BASE} is the base temperature. $(T_{MAX} + T_{MIN})/2$ was replaced by daily average temperature. Cultivation practices in each year are shown in Table 2.2. T_{BASE} was determined so as to minimize an estimation error, as described later.

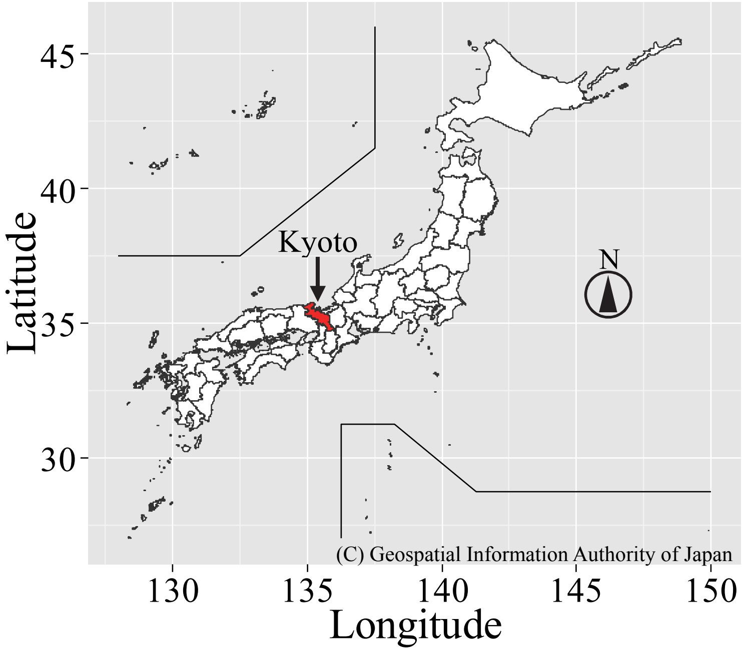

Created by the author based on National Land Numerical Information (Geospatial Information Authority of Japan) (http://nlftp.mlit.go.jp/ksj/gml/datalist/KsjTmplt-N03.html)

Fig. 2.1 Location of Kyoto Prefecture (red part)

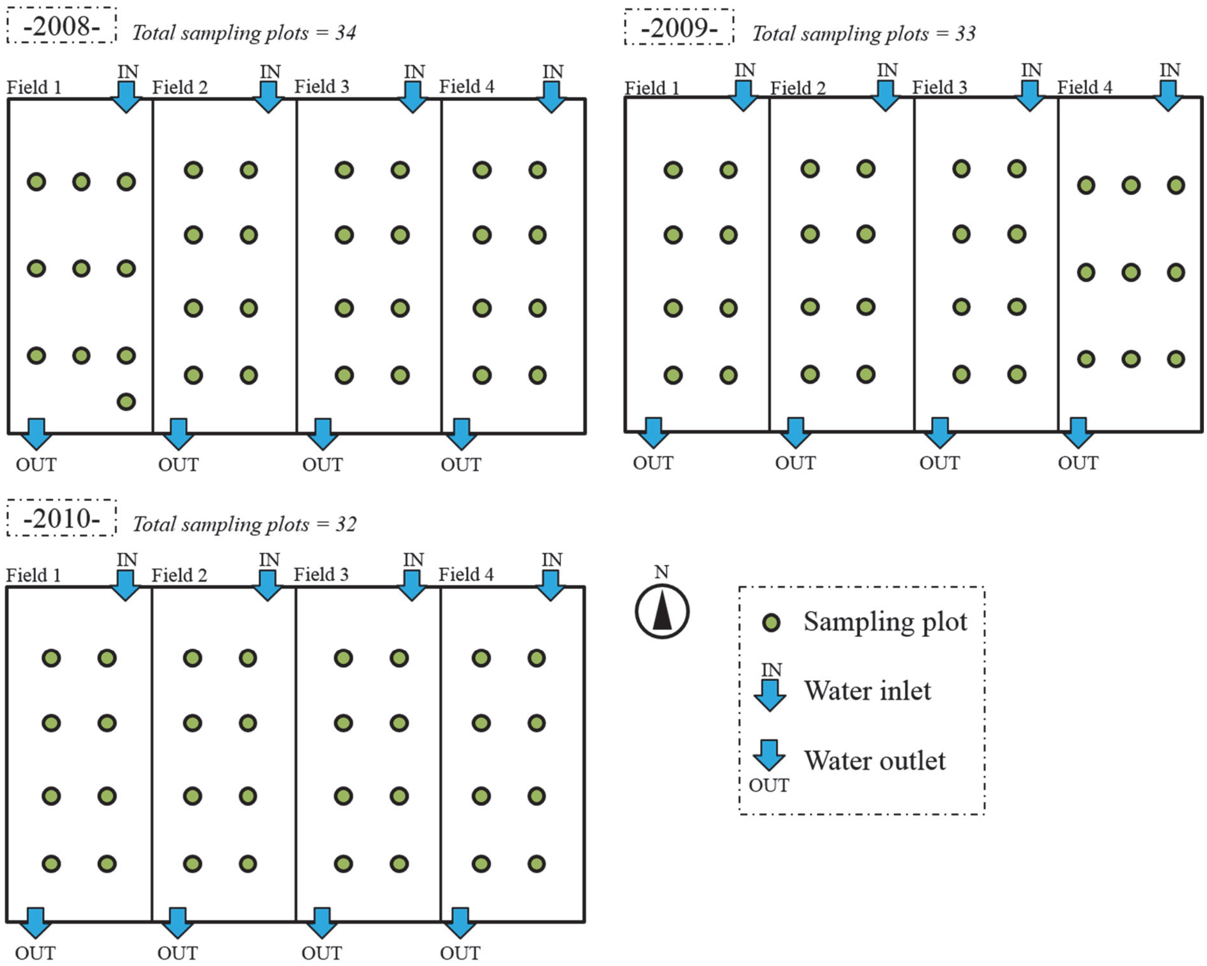

Fig. 2.2 Plot arrangement for 3 years

Table 2.1 Nitrogen treatment in each field for 3 years

Field	Area (ha)	2008		2009		2010	
		Basal dressing (kg N/ha)	Top-dressing (kg N/ha)	Basal dressing (kg N/ha)	Top-dressing (kg N/ha)	Basal dressing (kg N/ha)	Top-dressing (kg N/ha)
1	0.23	65	68	63	78	72	55
2	0.26	60	68	61	80	70	53
3	0.21	45	76	65	83	73	55
4	0.22	48	74	77	79	75	53
Total	0.92						

Table 2.2 Field management

	2008	2009	2010
Management date			
Transplanting	25 May	24 May	27 May
Sampling at panicle initiation stage	16 July	19 July	26 July
Image acquisition	16 July	19 July	26 July
Day after transplanting [a]	52	56	60
Sum of GDD (°C-day) [b]	597	659	741
Sampling at heading stage	13 August	11 August	16 August
Image acquisition	12 August	10 August	15 August
Day after transplanting	80	79	81
Sum of GDD (°C-day)	1117	1046	1155
Sampling before harvest	10 September	14 September	17 September
Image acquisition	10 September	14 September	17 September
Day after transplanting	108	113	113

[a] Day from transplanting to sampling

[b] Sum of the daily average temperature minus 10°C from transplanting to sampling

2.2 Hyperspectral imaging system

Figure 2.3 shows the experimental set-up for a ground-based hyperspectral imaging system. All images were taken at each important growing stage (at panicle initiation, at heading, just before harvest) using a hyperspectral camera (ImSpector QE V10E, Specim, Oulu, Finland) (Table 2.3) that was placed approximately 2 m above the rice canopy. The system consisted of a prism-grating-prism (PGP) component and a monochrome camera (C8484-05G, Hamamatsu Photonics K. K., Hamamatsu, Japan). The slit width and length of the PGP were 50 μm and 9.8 mm, respectively. The nominal spectral range was 400 to 1000 nm, with a 5-nm nominal spectral resolution. The spatial and spectral pixels in the image frame were 1344 and 1024, respectively. A C-mount lens (Cosmicar, f = 16 mm, 1:1.4) was installed in the front of the camera. The aperture was set to F/2.8, and the focus was fixed to 2 m during image acquisition. The hyperspectral camera is a line scan camera. In spatial scanning, spatial-spectral two-dimension images were collected line by line through rotational movement of the camera via a motor. The camera was connected to a planetary gearbox and motor (TAM72001; Tamiya, Inc., Shizuoka, Japan) for the constant control of camera angular speed. Hyperspectral images were acquired between 10:00 to 14:00 to reduce the influence of the incident light angle and dew on the leaf surfaces. Reference boards (gray panels) were placed on either side of the rice plant canopy to correct for changes in the intensity of the incoming light during image acquisition.

Images were acquired by a digital camera controller (Gnome IEEE-1394, Coriander version 1.0.1, Damien Douxchamps). Sensor sensitivity was manually controlled via Coriander software to stop it from becoming saturated by changes in incoming light intensity during image acquisition. After the scans were completed, the spatial-spectral matrices were combined to construct a three-dimensional spatial and spectral data cube (Fig. 2.4). The spatial resolution of the images was approximately 1 × 1 mm at 2 m above the rice canopy. Figure 2.5 shows a flow chart of the data processing.

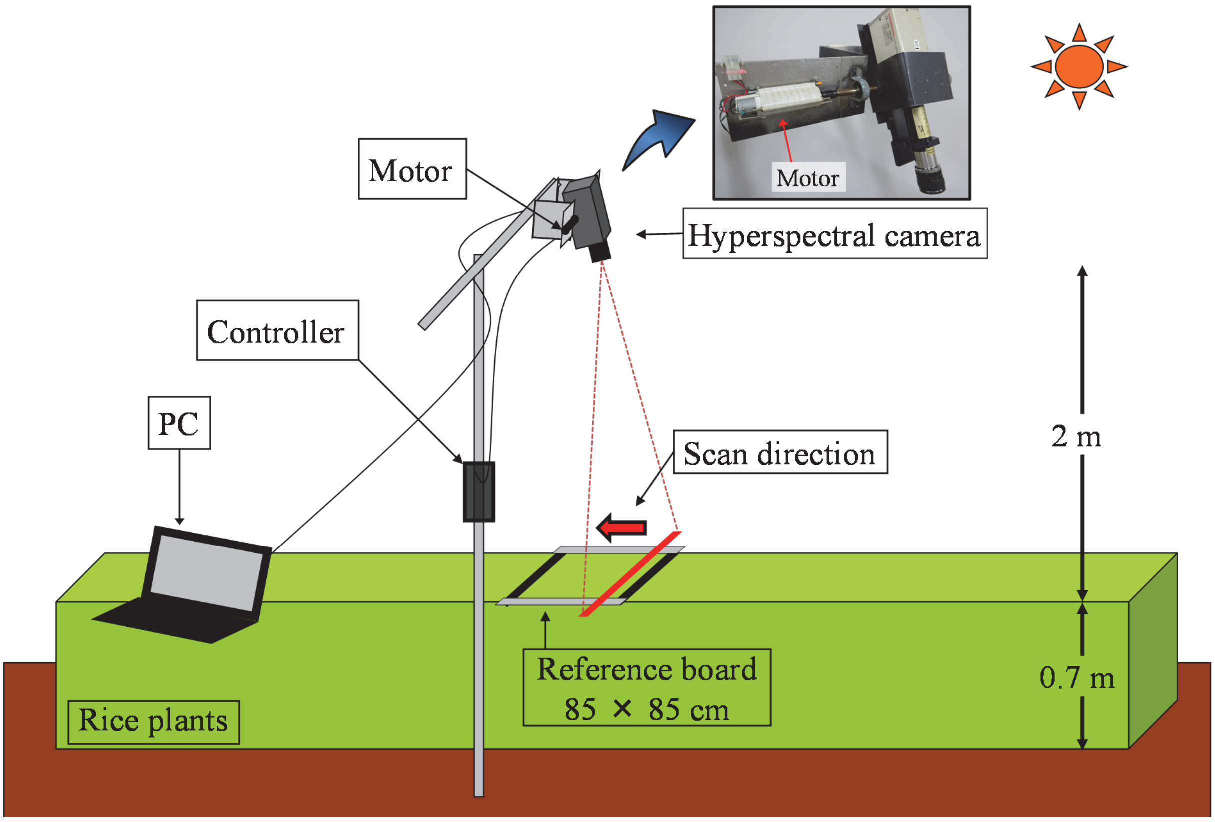

Fig. 2.3 Ground-based hyperspectral imaging system

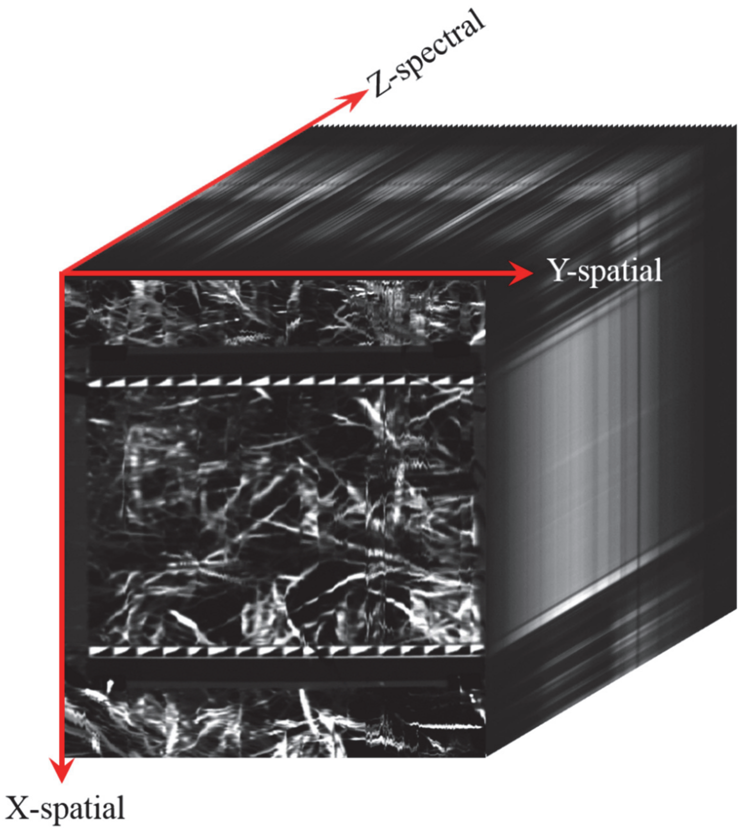

Fig. 2.4 Three-dimensional hyperspectral data cube

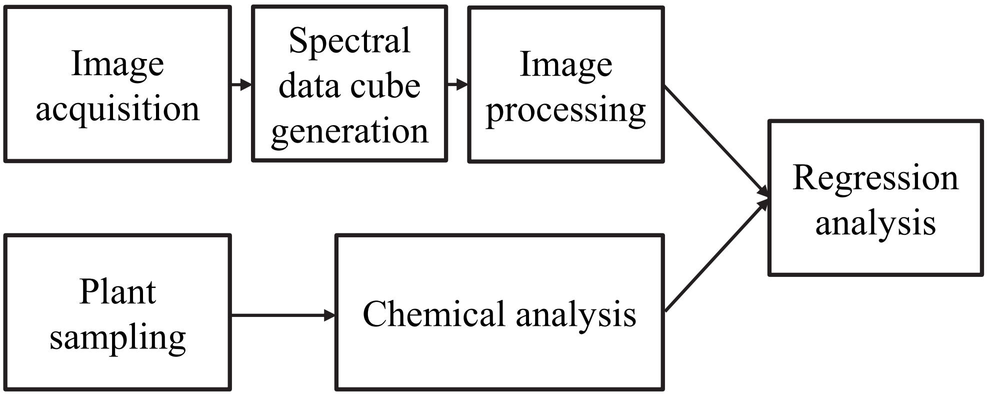

Fig. 2.5 Hyperspectral data processing flow

Table 2.3 Specification of the Specim hyperspectral camera

Specim QE-V10E	
Camera model	Hamamatsu C8484-05G, S.N520335
Camera sensor	2/3" CCD, 1344×1024 pixels, 2×2 binning
Filters	OG-515, OG-590, LPF1300, LPF1400
Input slit size (width/length)	50μm / 9.8mm
Nominal spectral range	400nm – 1000nm
Nominal spectral resolution	5nm
Numerical aperture	F/2.8
Nominal spatial bending	< ±2.75nm

2.3 Image processing

2.3.1 At panicle initiation stage and heading stage

Images were analyzed using the Environment for Visualizing Images (ENVI) software (version 5.0; ITT Visual Information Solutions, Boulder, Colorado, USA). Each image was separated into 2 parts: (1) the rice plant (leaves and stems) and (2) other elements (e.g., ponding water, soil background) by the $GNDVI-NDVI$ value, as shown in equation (2.2). The $GNDVI-NDVI$ image was used to obtain the rice canopy reflectance which is composed of leaves and the upper part of the stems.

$$GNDVI-NDVI=\frac{DN_{NIR}-DN_{green}}{DN_{NIR}+DN_{green}}-\frac{DN_{NIR}-DN_{red}}{DN_{NIR}+DN_{red}} \tag{2.2}$$

where, *DN* represents the digital number of the near-infrared (NIR) (845 nm), green (564 nm), or red (668 nm) spectrum, indicating the brightness of each spectrum.

Figure 2.6 shows a composite RGB image (a), grayscale *GNDVI−NDVI* image (b), and region of interest (ROI) in the *GNDVI−NDVI* image based on a threshold value of *GNDVI−NDVI* (c) at panicle initiation stage. The composite RGB image was constructed with the red (668 nm), green (564 nm) and blue (473 nm) spectrum of the hyperspectral data cube. In the *GNDVI−NDVI* image, gray or black colored areas correspond to the rice plants, while white colored areas correspond to the ponding water or soil background. The threshold value was manually set to select only the rice plant area in each image. The threshold values ranged from −0.20 to −0.10. In Fig. 2.6(c), rice plant is represented as red and reference board is represented as blue. Red part satisfies the *GNDVI−NDVI* values ≤ the threshold value and within the target sampling area. Blue part was specified with a mouse.

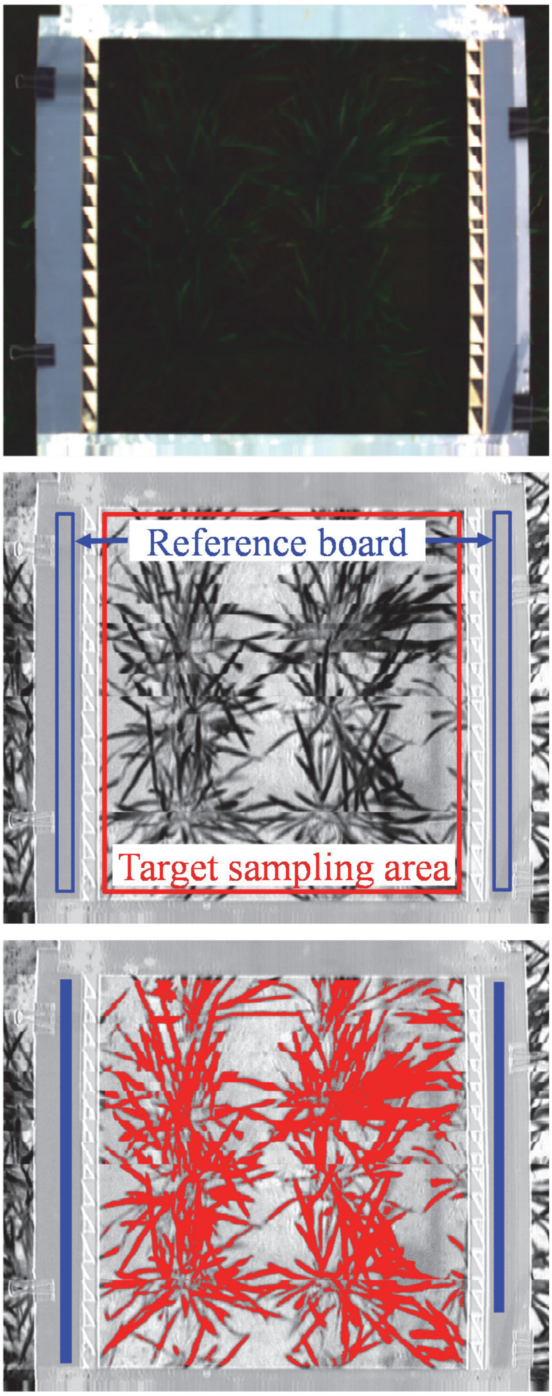

(a)
(b)
(c)

Fig. 2.6 Sample image of rice plants at panicle initiation stage : RGB (a), *GNDVI−NDVI* (b), and ROI (c)

Similarly, Fig 2.7 shows a composite RGB image (a), grayscale *GNDVI−NDVI* image (b), and region of interest (ROI) in the *GNDVI−NDVI* image based on a threshold value of *GNDVI−NDVI* (c) at heading stage. The method of setting the threshold value to select only the rice plant area was same as that at the panicle initiation stage. The threshold values ranged from −0.12 to −0.10.

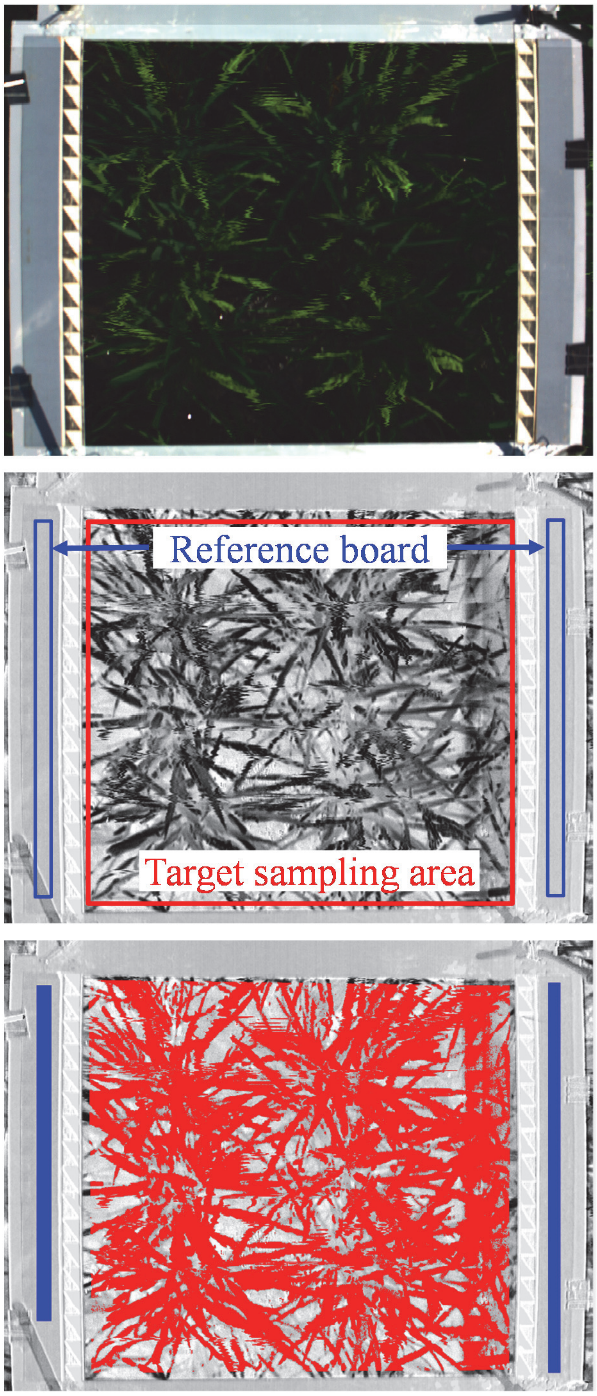

(a)

(b)

(c)

Fig. 2.7 Sample image of rice plants at heading stage: RGB (a), *GNDVI−NDVI* (b), and ROI (c)

The reflectance of the rice plant (ROI_RICE; red color) and the reflectance of the reference board area (ROI_BOARD; blue color) were extracted using the ROI function of the ENVI software. Then, we obtained 1024 spectral datasets of rice and the reference boards. Rice plant reflectance (Ref_{RICE}) was calculated using the ratio of the mean value of rice plant area reflectance to that of the reference board area, as shown in equation (2.3).

$$Ref_{RICE} = \frac{DN_{ROI\_RICE}}{DN_{ROI\_BOARD}} \tag{2.3}$$

where, Ref_{RICE} represents the rice plant reflectance and DN_{ROI_RICE} and DN_{ROI_BOARD} represent the mean values of the digital readings for rice plants and reference boards in the ROI.

2.3.2 Just before harvest

The acquired images were processed using mouse-based software written in Java. The reflectance of the five ROIs was obtained by segmenting the *R+G+B* and *GNDVI−NDVI* images. The five ROIs are: ROI-I; the overall target area, ROI-II; non-canopy area (stems and soil), ROI-III; canopy area (leaves, yellow leaves, and ears), ROI-IV; leaf area, and ROI-V; ear and yellow leaf area. Figure 2.8 shows a composite RGB image (a), grayscale *R+G+B* image (b), and grayscale *GNDVI−NDVI* image (c) just before harvest. The composite RGB image was constructed with the red (680 nm), green (566 nm) and blue (473 nm) spectrum of hyperspectral data cube. *R+G+B* and *GNDVI−NDVI* images, which are respectively calculated as follows.

$$R + G + B = DN_{RED} + DN_{GREEN} + DN_{BLUE} \tag{2.4}$$

$$GNDVI - NDVI = \frac{DN_{NIR} - DN_{GREEN}}{DN_{NIR} + DN_{GREEN}} - \frac{DN_{NIR} - DN_{RED}}{DN_{NIR} + DN_{RED}} \tag{2.5}$$

where *DN* denotes the digital value of the brightness of the red (680 nm), green (566 nm), blue (473 nm), or NIR (750 nm) spectra.

In the *R+G+B* image, the area of gray or white corresponds to the rice canopy (Fig. 2.8, b), which consists of leaves and ears in the upper layer. As can be seen in Fig. 2.8 (c), the colors of the leaf and ear pixels are clearly different from each other in the *GNDVI−NDVI* image, namely, the color of the ears are lighter and that of the leaves is black. Figure 2.9 shows a histogram of the *R+G+B* values within ROI-I. The *R+G+B* histogram was used to separate ROI-II (non-canopy area) from ROI-III (canopy area). When the rice plant gets close to harvesting time, the rice inclines in any direction because of the heavy ripened ears and strong winds. Therefore, it is necessary to obtain canopy reflectance, and an $R+G+B$ image is suitable for this aim. The $R+G+B$ threshold value is twice the interval from the first bin to the maximum frequency bin (Fig. 2.9) and was empirically determined. The $GNDVI-NDVI$ threshold value to separate ROI-IV from ROI-V was set to zero.

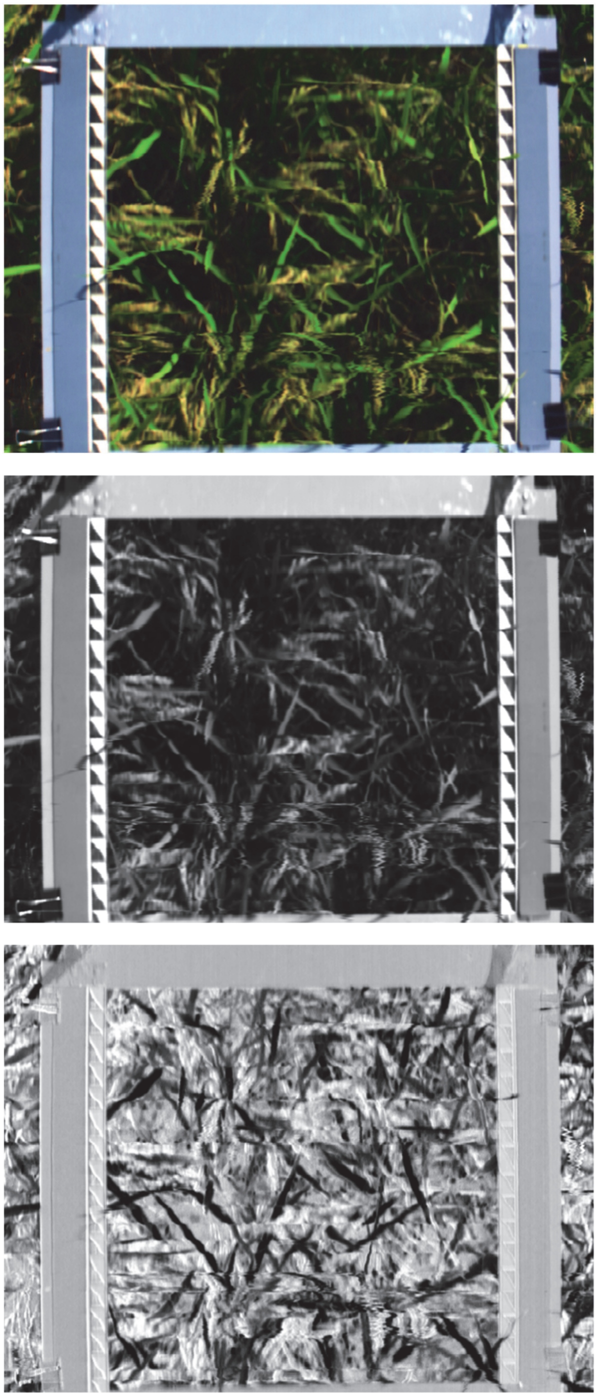

(a)

(b)

(c)

Fig. 2.8 Sample image of rice plants just before harvest: RGB (a), *R*+*G*+*B* (b), and *GNDVI*−*NDVI* (c)

To summarize, ROI-I is the inside of the reference board, namely, the target sampling area. ROI-II is the non-canopy area (i.e., the lower layer, such as stems, soil, and the less illuminated parts of the rice plants), ROI-III is the canopy area (i.e., the upper layer, such as leaves and ears), ROI-IV is the leaf area and ROI-V is the ear area. Table 2.4 shows a diagram summarizing the image processing. Finally, $Ref_{Corrected\_ROI}$ was calculated using the ratio of the reflectance of each ROI to that of the reference board area, as follows.

$$Ref_{Corrected\_ROI} = \frac{DN_{ROI}}{DN_{ROI\_BOARD}} \tag{2.6}$$

where DN denotes the digital brightness of spectra, $Ref_{Corrected\_ROI}$ represents the ROI reflectance corrected using the reference board, and DN_{ROI} and DN_{ROI_BOARD} represent the digital number of the ROI and reference board, respectively.

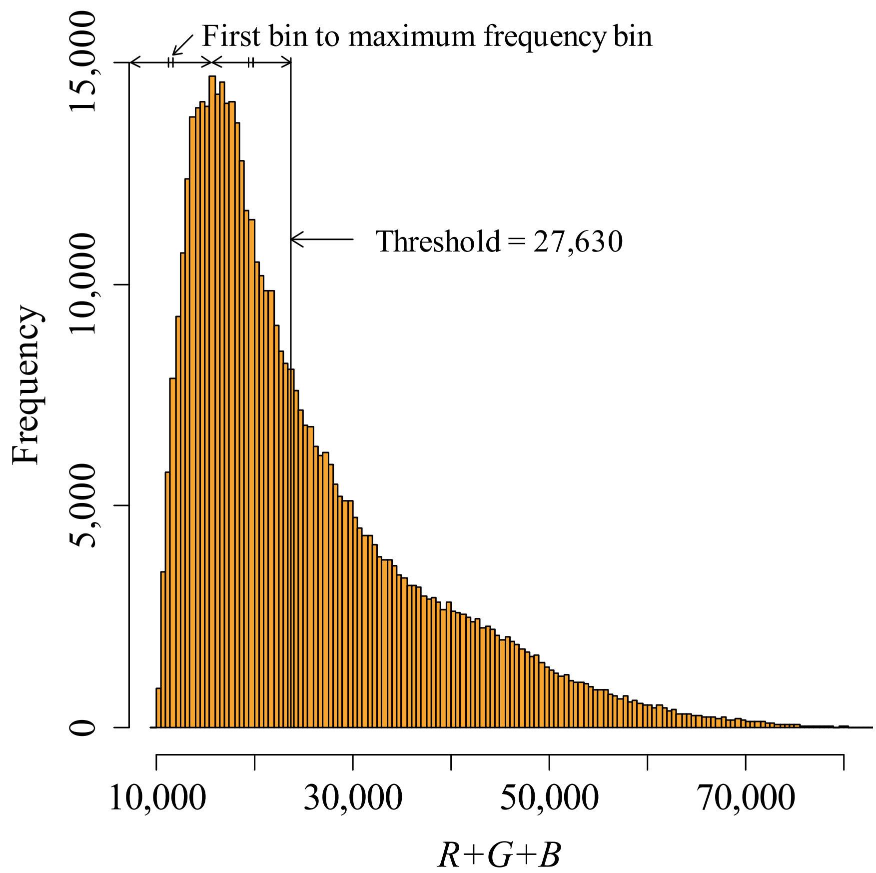

Fig. 2.9 *R+G+B* histogram at ROI-I

Table 2.4 Summary of five ROIs

ROI	Condition	Characteristics
I	Manual selection	Target sampling area
II	ROI-I ∩ R+G+B < threshold	Non-canopy area
III	ROI-I ∩ R+G+B ≥ threshold	Canopy area
IV	ROI-III ∩ $GNDVI-NDVI$ < 0	Leaf area
V	ROI-III ∩ $GNDVI-NDVI$ ≥ 0	Ear area

The threshold was determined by histogram inspection

2.4 Physical sampling and measurement of rice

2.4.1 At panicle initiation stage

After the hyperspectral images were obtained, six rice plants without roots (aboveground biomass) were removed at each sampling point, and the ground areas occupied by the plants measured. The samples were then mixed and divided into two portions in a 1:2 ratio by weight. Samples from the smaller fraction were separated into leaves and stems, which were analyzed to determine the leaf-stem ratio and nitrogen concentration. All samples were dried in a forced convection drying oven at 80 °C for at least 72 h and then weighed. The respective dry mass of the leaves and stems from the larger fraction were calculated from those of the smaller fraction. The leaves and stems of the smaller fraction were finely ground using a pulverizing mill (TI-100; Cosmic Mechanical Technology Co., Ltd., Iwaki, Japan). The nitrogen concentration of each fraction was determined 3 times using a gas chromatography (SUMIGRAPH NC-22F; Sumika Chemical Analysis Service, Ltd., Tokyo, Japan). The nitrogen content at each sampling point was calculated as a product of the dry mass per unit area and the mean nitrogen concentration. Figure 2.10 shows the process of calculating the nitrogen content of rice plants.

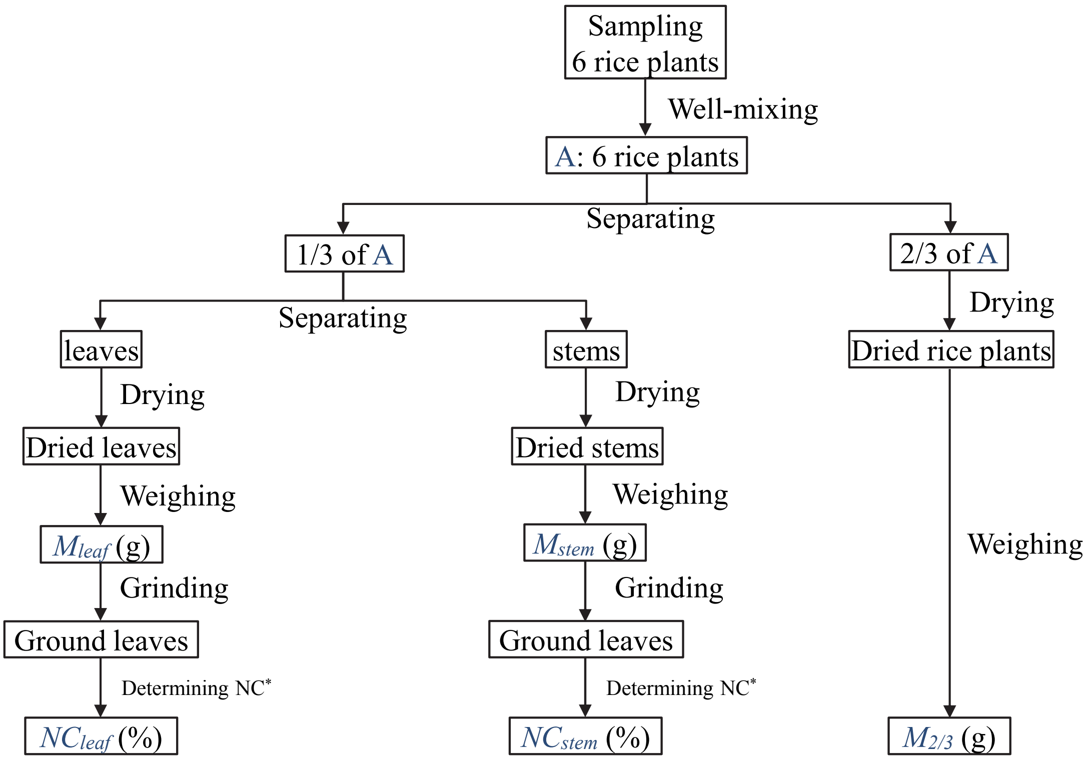

R_{leaf} : Leaf ratio (%) = $\frac{M_{leaf}}{M_{leaf}+M_{stem}} \times 100$

R_{stem} : Stem ratio (%) = $\frac{M_{stem}}{M_{leaf}+M_{stem}} \times 100$

$Area$: Sampling area (m^2)

$$\text{Nitrogen content (g/m}^2\text{)} = \frac{\frac{NC_{leaf}}{100}\times\left(M_{leaf}+M_{2/3}\times\frac{R_{leaf}}{100}\right)+\frac{NC_{stem}}{100}\times\left(M_{stem}+M_{2/3}\times\frac{R_{stem}}{100}\right)}{Area}$$

*: Nitrogen concentration

Fig. 2.10 Process of calculating nitrogen content of rice plants at panicle initiation stage

2.3.2 At heading stage

After the hyperspectral images were obtained, six rice plants without roots (aboveground biomass) were removed at each sampling point and the ground areas occupied by the plants measured. The samples were then mixed and divided into two portions in a 1:2 proportion by weight. Samples from the smaller fraction were separated into leaves, stems, and heads and were analyzed to determine their ratio and nitrogen concentration. All samples were dried in a circulating drying oven at 80°C for at least 72 h and then weighed. The respective dry masses of the leaves, stems, and heads from the larger fraction were calculated from those of the smaller fraction. The leaves and stems of the smaller fraction were finely ground using a pulverizing mill (TI-100; Cosmic

Mechanical Technology Co., Ltd., Iwaki, Japan). The nitrogen concentration of each fraction, except for the head fractions, was determined three times by a gas chromatography (SUMIGRAPH NC-22F; Sumika Chemical Analysis Service, Ltd., Tokyo, Japan). The nitrogen content at each sampling point was calculated as a product of the dry mass per unit area and the mean nitrogen concentration. Figure 2.11 shows process of calculating the nitrogen content of rice plants.

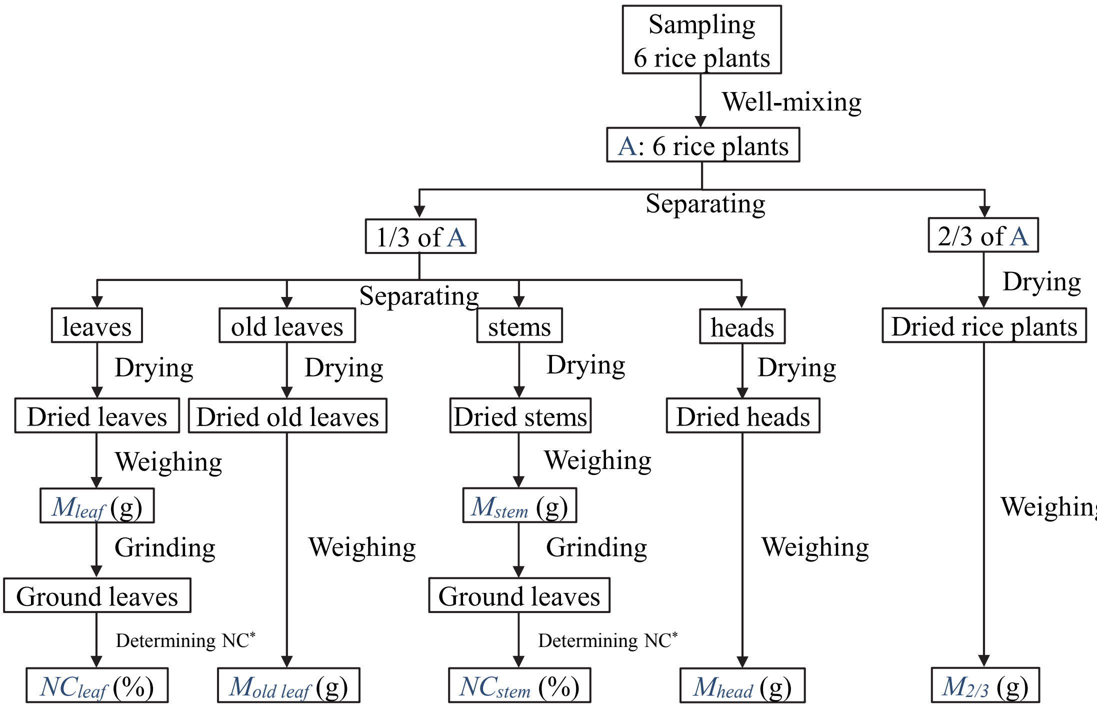

R_{leaf} : Leaf ratio (%) $= \frac{M_{leaf}}{M_{leaf}+M_{old\,leaf}+M_{stem}+M_{head}} \times 100$

R_{stem} : Stem ratio (%) $= \frac{M_{stem}}{M_{leaf}+M_{old\,leaf}+M_{stem}+M_{head}} \times 100$

$Area$: Sampling area (m^2)

$$\text{Nitrogen content (g/m}^2\text{)} = \frac{\frac{NC_{leaf}}{100}\times\left(M_{leaf}+M_{2/3}\times\frac{R_{leaf}}{100}\right)+\frac{NC_{stem}}{100}\times\left(M_{stem}+M_{2/3}\times\frac{R_{stem}}{100}\right)}{Area}$$

*: Nitrogen concentration

Fig. 2.11 Process of calculating nitrogen content of rice plants at heading stage

2.3.3 Just before harvest

After the hyperspectral images were obtained, eight rice plants were harvested at each sampling point. The samples were threshed and dried to about 15% moisture content. Afterward, they were husked and sorted with a 1.9 mm mesh sieve. The protein content of the brown rice (200 cm^3) was measured using a rice grain taste analyzer (RCTA11A, Satake Co., Hiroshima, Japan and RLTA10A, Satake Co., Hiroshima, Japan). The RCTA11A was used for analyzing samples collected in 2008 and 2009, and the RLTA10A was used for analyzing samples collected in 2010. Both taste analyzers have the same performance. Figure 2.12 shows the process of measuring the protein content of brown rice.

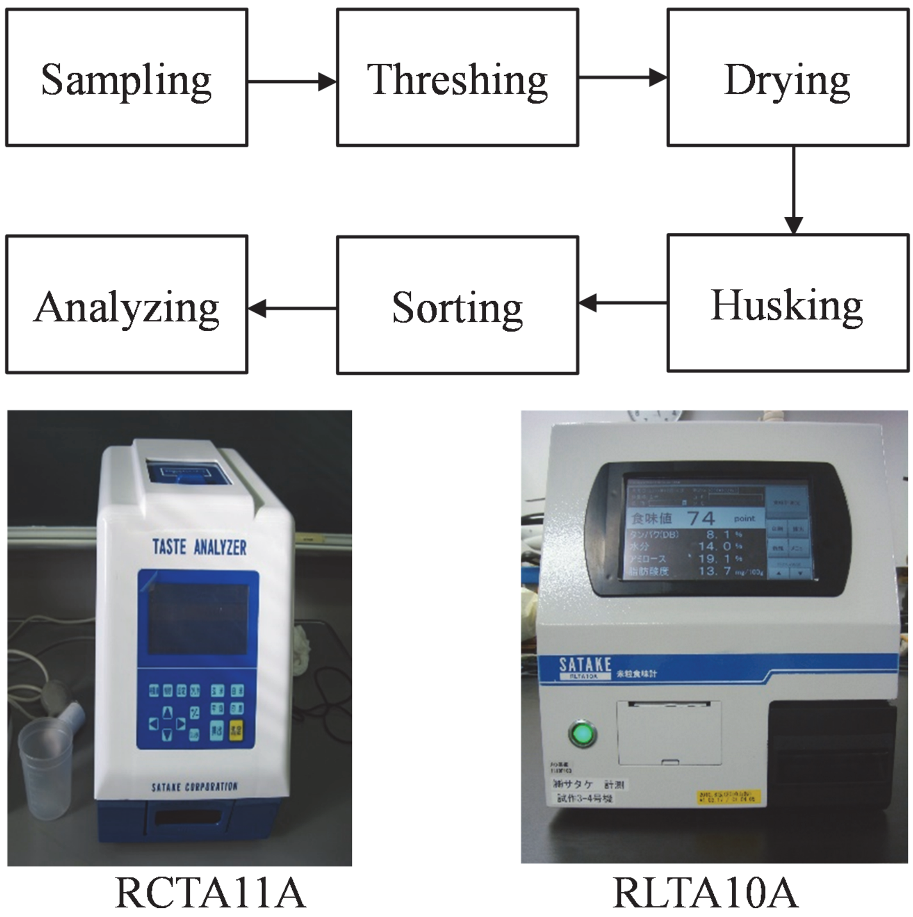

Fig. 2.12 Process of measuring protein content of brown rice before harvest

2.4 Statistical Procedures

A partial least squares regression (PLSR) model for the relationship between the corrected reflectance via reference board and the objective variable (nitrogen content or protein content of the rice plant) was generated using the statistics software R (version 3.0.3, R Foundation for Statistical Computing). All spectral bands were used for the establishment of the PLSR model. The model was calculated using a leave-one-out cross-validation to evaluate the quality of the calibration model. In this method, all samples except one were used to establish a calibration model that was then used to predict the remaining sample. The optimum number of latent variables was determined by the method of Osten (Osten, 1988), given by

$$F = \frac{PRESS_k - PRESS_{k+1}}{df_k - df_{k+1}} \Bigg/ \frac{PRESS_{k+1}}{df_{k+1}} \tag{2.7}$$

This criterion tests the significance of incremental changes in predicted residual sum of squares (*PRESS*) using an *F*-test. Here, $PRESS_k$ denotes the $PRESS$ after including the first k latent variables and df_k is the degree of freedom of $PRESS_k$. The criterion is compared against $F(df_k - df_{k+1}, df_{k+1}; 0.95)$. This method may provide a more robust performance than the local minimum in the $PRESS$ method. The performance of the model was evaluated using the coefficient of determination R^2, the root mean square error of prediction (*RMSE*) as the indicators of the average error of analysis, respectively calculated as follows:

$$PRESS = \sum_{i=1}^{n} (y_i - \hat{y}_i)^2 \tag{2.8}$$

$$R^2 = 1 - \frac{\sum_{i=1}^{n} (y_i - \hat{y}_i)^2}{\sum_{i=1}^{n} (y_i - \bar{y})^2} \tag{2.9}$$

$$RMSE = \sqrt{\frac{1}{n} \sum_{i=1}^{n} (y_i - \hat{y}_i)^2} \tag{2.10}$$

In addition, the relative error (*RE*), which represents the ratio of *RMSE* to the mean value for the protein content, was also used. Calculated as follows.

$$RE = \frac{100}{\bar{y}} \sqrt{\frac{1}{n} \sum_{i=1}^{n} (y_i - \hat{y}_i)^2} \tag{2.11}$$

where, y_i, $\hat{y}_i$, and $\bar{y}$ are the measured, predicted, and mean values of the nitrogen contents, respectively, and n is the number of samples.

A relationship between reflectance of rice plant and its nitrogen content was modeled with PLS regression, as shown in (2.12). The GDD integrated model was constructed, based on the association between rice nitrogen content and GDD, as well as reflectance, as shown in (2.13). The GDD integrated model was expected to improve the accuracy of mutual estimation by reducing the influence of the growing condition.

$$\hat{y}_i = b_0 + \sum_{k=1}^{1024} b_k x_{ik} \tag{2.12}$$

$$\hat{y}_i = b_0 + \sum_{k=1}^{1024} b_k x_{ik} + b_{1025}\, g_{dd\_t} \tag{2.13}$$

where, $\hat{y}_i$, is the predicted values of the nitrogen content and b_0 is the intercept and b_k and b_{1025} are the PLSR coefficients for a model with optimum number of latent variables. x_{ik} is the reflectance of the k-th spectral band and g_{dd_t} is GDD under the base temperature t.

References

McMaster, G. S., and W. Wilhelm. 1997. Growing degree-days: one equation, two interpretations. *Agricultural and Forest Meteorology* 87(4):291-300.

Osten, D. W. 1988. Selection of optimal regression models via cross‐validation. *Journal of Chemometrics* 2(1):39-48.

Chapter III

Estimation of Nitrogen Content at Panicle Initiation Stage

Abstract Ground-based hyperspectral imagery was applied to rice plants at panicle initiation stage to estimate their nitrogen content. A partial least squares regression (PLSR) model that incorporated both the reflectance and growing degree-days (GDD) to account for differences in growing temperature conditions across a 3-year period was developed. The acquired images were divided into two components: (1) the rice plant and (2) other elements (e.g., ponding water, soil background) by using the *GNDVI−NDVI* equation. Rice plant reflectance (Ref_{RICE}) was calculated as the ratio of rice plant reflectance to that of a reference board. Three types of PLSR models were constructed: 1-year, 2-year, and 2-year GDD. Mutual estimation was used to infer the predictive power of the three models, which was calculated by estimating the values for the other years. The root mean square error of prediction (*RMSE*) of the mutual estimation for the 1-year and 2-year PLSR models was high because of overestimation and underestimation. In contrast, the *RMSE* of the mutual estimation for the 2-year GDD PLSR models clearly decreased. It was inferred that hyperspectral imaging from 400 to 1000 nm could not predict variation in the amount of growth caused by weather variation expressed as GDD. This study indicates that the combination of reflectance and temperature data could be used to potentially construct an adaptable model to identify variance in growing conditions.

Keywords Ground-based hyperspectral imaging · Nitrogen content · Paddy rice · Panicle initiation stage · Growing degree-days · Growing degree-days integrated model

3.1 Introduction

Nitrogen is an essential plant nutrient that accounts an economically large input cost for farmers in rice cultivation (Bajwa et al., 2010). In rice cultivation, nitrogen is applied as a topdressing at panicle initiation stage to increase rice grain yield in Japan (Inamura, 2003). Hence, it is important to calculate the nitrogen content of the rice plant at this stage so as to be able to place the optimum amount of topdressing (Ozaki et al., 2012). The nitrogen content of rice plants differs drastically among and within fields. Moreover, existing chemical analysis methods used to quantify nitrogen content are destructive, laborious, and time-consuming. Hence, to optimize agricultural management decisions, a non-destructive, quick, and reliable method is required.

Various applications of remote sensing have been investigated by many researchers. This research suggests the ability of this technique to predict crop biochemical or physiological properties nondestructively using crop canopy reflectance could fulfill the demand for a non-destructive measurement tool. At present, two approaches are used in precision agriculture, namely, (1) the development of vegetation indices, such as the normalized difference vegetation index (NDVI), (Oppelt and Mauser, 2004; Rouse Jr et al., 1974; Tucker, 1979; Xue et al., 2004) and (2) models based on regression analysis (Nguyen and Lee, 2006; Wang et al., 2011). In addition, regression analysis based on several vegetation indices has been studied (Bajwa et al., 2010). The PLSR model has desirable properties that improve the precision of modeling parameters as the number of relevant variables and observations increase (Wold et al., 2001). PLSR analysis is one of the most efficient methods used to extract and create reliable models in a wide range of fields (Nguyen and Lee, 2006). Hence, PLSR might prove useful as an exploratory and predictive tool when applied to hyperspectral reflectance data (Hansen and Schjoerring, 2003).

It can be difficult to estimate the nitrogen content of rice plants at the panicle initiation stage using remote sensing techniques. Because leaf color obtained by remote sensing relates to not the amount of nitrogen but to the concentration of nitrogen. From a practical standpoint, an estimation model should have the ability to estimate crop status from new remote-sensing data with a certain level of precision or accuracy. (Ryu et al., 2009, 2011) suggested that remote sensing models may be affected by differences in environmental variables, such as weather conditions. Growing degree-day (GDD) is calculated from the air temperature measurements and represents a weather condition that is frequently used to describe the timing of biological processes (McMaster and Wilhelm, 1997). Went showed that GDD constrains the developmental rate of plants, rather than the growth rate (Went, 1953). However, GDD does indirectly influence the amount of growth. For instance, the sooner the tillering stage begins, due to a relatively high GDD, the higher the increase in the number of leaves on the main axis (the amount of growth). Thus, I proposed a model based on a combination of both reflectance and GDD. To my knowledge, previous studies have not used hyperspectral imaging with a GDD to develop an estimation model of nitrogen content in rice at panicle initiation stage.

Therefore, this study aimed to construct a model that considered GDD over a 3-year period. The specific research objectives were (1) to establish a PLSR model to determine nitrogen content at panicle initiation stage using ground-based hyperspectral imaging, (2) to suggest an appropriate GDD integrated model that worked across years, and (3) to compare the accuracy of conventional models and the suggested GDD integrated model.

3.2 Materials and methods

3.2.1 Image processing

Images were analyzed using the Environment for Visualizing Images (ENVI) software (version 5.0; ITT Visual Information Solutions, Boulder, Colorado, USA). See section 2.3.1 for details.

3.2.2 Rice plant sampling and chemical analysis

See section 2.4.1.

3.3 Results and Discussion

3.3.1 Measurement of vegetation data and canopy reflectance

Table 3.1 shows the measured nitrogen content at panicle initiation stage for the 3-year study period. Because of strong wind during image acquisition, some images were unusable and, therefore, were excluded from the analysis. Thus, the number of images acquired was 24, 27, and 26 in 2008, 2009, and 2010, respectively. The mean nitrogen content values ranged from 2.67 to 5.43 g/m^2 in 2008, 5.70 to 6.96 g/m^2 in 2009, and 7.38 to 8.02 g/m^2 in 2010. The differences among years were significant (P < 0.001; ANOVA). Multiple comparisons indicated that there were significant differences in the mean nitrogen content values among 2008, 2009, and 2010, with a 5% level of significance. This result indicates that 2010 had the greatest amount of vegetation among the 3 years.

Table 3.1 Summary of nitrogen content (g/m²) in rice plant at panicle initiation stage

Field	2008			2009			2010		
	n	Mean (g/m²)	SD	*n*	Mean (g/m²)	SD	*n*	Mean (g/m²)	SD
1	5	2.67	0.61	7	5.70	0.82	6	7.38	1.06
2	6	5.43	1.54	5	6.96	0.38	6	7.89	1.16
3	8	4.77	1.62	7	6.26	0.86	6	8.02	1.10
4	5	3.52	1.08	8	5.83	0.67	8	7.50	0.76
Total	24	4.24	1.64	27	6.12	0.82	26	7.68	0.98

n: number of samples, SD: standard deviation

Figure 3.1 shows the mean reflectance of a rice plant (Ref_{RICE}), which was extracted by *GNDVI−NDVI*. The value of reflectance on the Y-axis was more than one because of the use of the gray color reference board. The reflectance of a rice plant exhibited limited variation in the visible region, but was variable in the NIR region. This result is in accordance with previous observations (Hansen and Schjoerring, 2003; Nguyen and Lee, 2006; Xue et al., 2004).

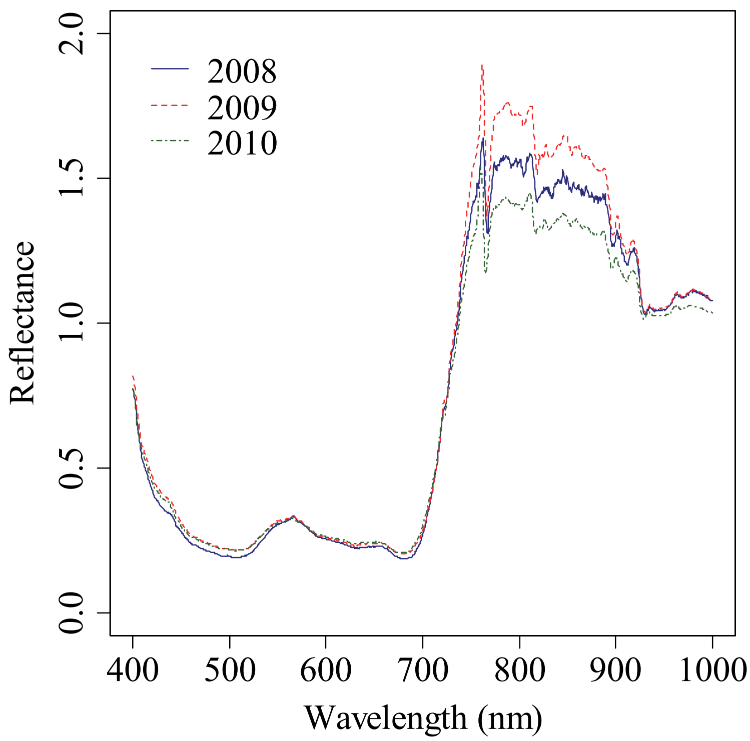

Fig. 3.1 Rice plant reflectance at panicle initiation stage

3.3.2 Performance of the one-year PLSR model

In the current study, hyperspectral reflectance was related to the nitrogen content of rice plants at panicle initiation stage using PLSR analysis. Validation by *RMSE* ranged from 0.48 to 0.65 (Table 3.2). Compared to the calibration results, the *RMSE* and *RE* validation ranges were slightly higher; however, these 1-year models were considered to have good practical accuracy. Then the mutual estimation of each 1-year PLSR model was calculated using the data from the other years, as the test set to determine the utility of the model adaptability for the data collected in different years. In the mutual estimation with the 1-year PLSR models, the *RMSE* ranged from 0.49 to 3.95 g/m^2, while the *RE* ranged from 8.0 to 85% (Table 3.2). The mutual estimation *RMSE* and *RE* values were much higher than those obtained from the validation. The best mutual estimation result was obtained by estimating the 2009 data from the 2008 1-year PLSR model; whereby, the *RMSE* and *RE* were 0.49 g/m^2 and 8.0%, respectively. However, when the 2008 data was estimated from the 2010 1-year PLSR model, the *RMSE* and *RE* values were 3.60 g/m^2 and 85%, respectively. Figure 3.2 shows the relationships between the measured and estimated nitrogen content for the mutual estimation. When the 2010 1-year PLSR model was used to estimate the 2008 and 2009 data, both data were overestimated (Fig. 3.2, left bottom). In contrast, when the 2008 1-year PLSR model and 2009 1-year PLSR model were used to estimate the 2010 data, it was underestimated. For model adaptability (i.e., use for different years), it is desirable to narrow the distance between the measured and estimated 1:1 lines.

3.3.3 Performance of the two-year PLSR model

In the mutual estimation with the 1-year PLSR models, the *RMSE* and *RE* values were much higher than the validation values because of overestimation and underestimation, as shown in Fig. 3.2, left. In the model calibration, for the purpose of model adaptability, data are often collected under varying nitrogen fertilization, irrigation, planting density, cultivar, and weather conditions. Accordingly, the PLSR models based on data from 2 years (the 2-year PLSR model) were constructed to account for variation in growing conditions among years. Table 3.2 also shows the results of the calibration, leave-one-out cross validation, and mutual estimation with the 2-year PLSR models. The validation ranges of the *RMSE* and *RE* values were 0.51 to 0.80 g/m^2 and 9.8 to 13%, respectively. When the 2010 data were estimated from the 2-year PLSR model based on 2008 and 2009 data, the *RMSE* and *RE* were 3.32 g/m^2 and 43%, respectively. Thus, the accuracy was slightly superior to that of mutual estimation with the 2008 or 2009 1-year PLSR models. When the 2009 or 2008 data were estimated by the 2-year PLSR models based on the data of the other years (2008 and 2010 or 2009 and 2010), the *RMSE* and *RE* were superior to the worst result of the mutual estimation with the 1-year PLSR models. However, the data were still underestimated or overestimated by the 2-year PLSR models, as shown in Fig. 3.2, middle. These results may indicate that there are no significant differences in the accuracy between the 1- and 2-year PLSR models.

Table 3.2 Results of the calibration, leave-one-out cross validation, and mutual estimation analyses with the 1-year, 2-year, and 2-year GDD integrated PLSR models

Model type	Calibration						Validation			Mutual estimation			
	Data	*n*	LVs	R^2	*RMSE*	*RE*	R^2	*RMSE*	*RE*	Data	*n*	*RMSE*	*RE*
1-year reflectance	2008	24	3	0.92	0.46	11	0.84	0.65	15	2009	27	0.49	8.0
1-year reflectance	2008	24	3	0.92	0.46	11	0.84	0.65	15	2010	26	3.41	44
1-year reflectance	2009	27	4	0.85	0.31	5.1	0.65	0.48	7.9	2008	24	0.87	20
1-year reflectance	2009	27	4	0.85	0.31	5.1	0.65	0.48	7.9	2010	26	3.74	49
1-year reflectance	2010	26	4	0.90	0.31	4.0	0.69	0.54	7.0	2008	24	3.60	85
1-year reflectance	2010	26	4	0.90	0.31	4.0	0.69	0.54	7.0	2009	27	3.95	65
2-year reflectance	2008, 2009	51	4	0.92	0.43	8.2	0.89	0.51	9.8	2010	26	3.32	43
2-year reflectance	2008, 2010	50	4	0.91	0.64	11	0.88	0.76	13	2009	27	1.29	21
2-year reflectance	2009, 2010	53	4	0.73	0.61	8.9	0.55	0.80	12	2008	24	1.82	43
2-year reflectance + GDD	2008, 2009	51	4	0.92	0.44	8.4	0.89	0.52	10	2010	26	0.95	12
2-year reflectance + GDD	2008, 2010	50	4	0.95	0.50	8.4	0.92	0.62	10	2009	27	0.50	8.2
2-year reflectance + GDD	2009, 2010	53	4	0.82	0.50	7.3	0.72	0.63	9.1	2008	24	0.55	13

n: number of samples, LVs: number of latent variables, R^2: coefficient of determination, *RMSE*: root mean square error (g/m^2), *RE*: relative error (%)

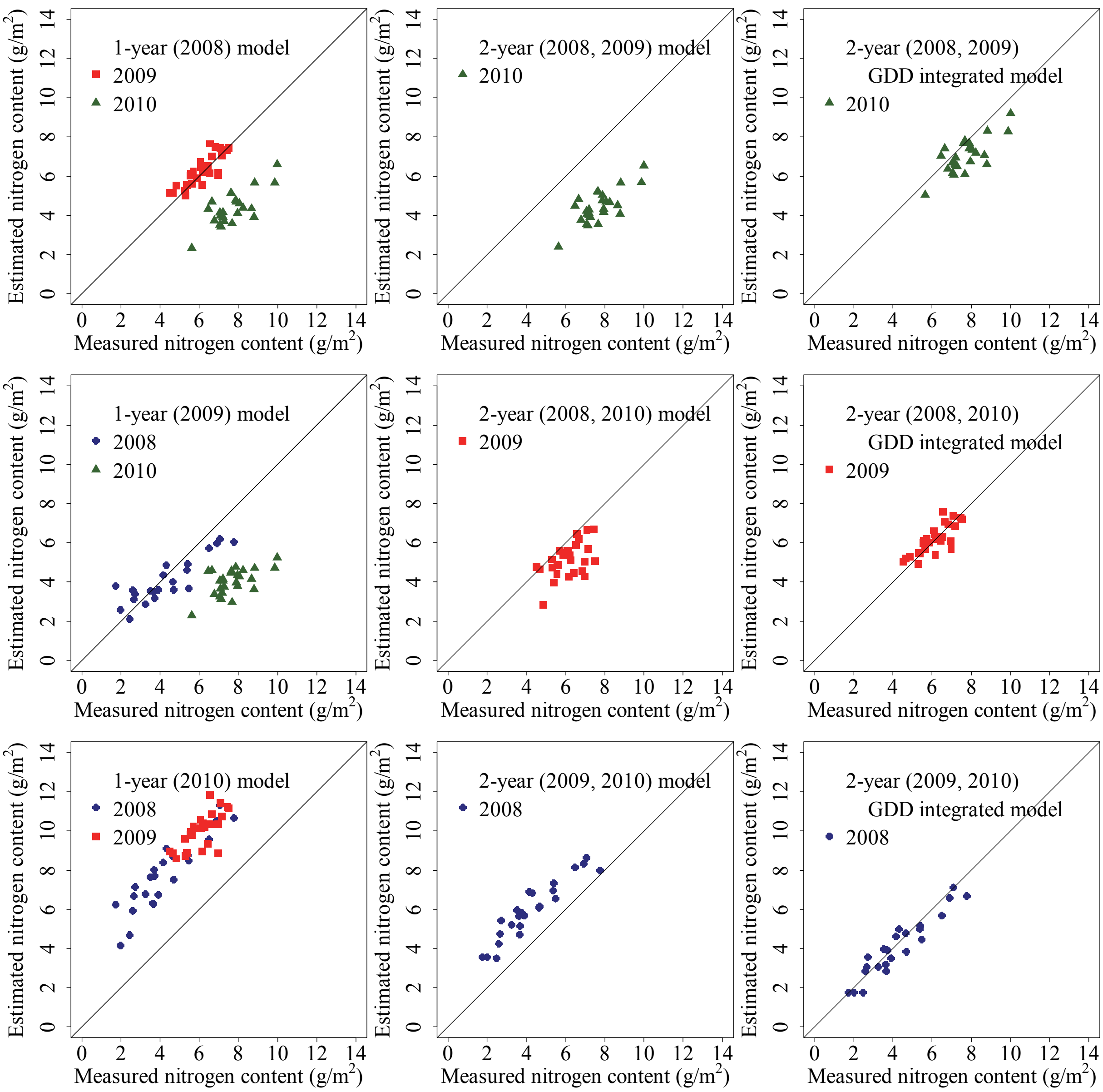

Fig. 3.2 Results of the mutual estimation with the 1-year (left), 2-year (middle), and 2-year GDD integrated (right) PLSR models

3.3.4 Performance of the two-year GDD integrated PLSR model

The mutual predictions data tended to be overestimated or underestimated by the 1- and 2-year PLSR models, with large and small GDD values (Table 2.2) tending to follow these overestimates and underestimates. Specifically, the 1-year PLSR models constructed under relatively high GDD values tended to overestimate relatively low GDD data. In contrast, 1-year PLSR models constructed under relatively low GDD values tended to underestimate relatively high GDD data.

These observations indicate that temperature data could be used to correct the influence of GDD differences among years. Furthermore, these observations demonstrated that remote sensing using ground-based hyperspectral imaging from 400 to 1000 nm could not be used to explain the intercept, which is the distance from the 1:1 line to the slope of the estimated values. Therefore, the indirect influence of GDD on the growth rate could be quantified to improve the accuracy of the mutual estimation. Accordingly, the number of latent variables (LVs) for the 2-year PLSR models was fixed at the number used for the 2-year PLSR models to quantify variation in the amount of growth due to variation in GDD. The incorporation of GDD data in the PLSR model required corresponding optimization. The GDD was calculated as the sum of the average daily temperature subtracted from a base temperature, to quantify the variation in the amount of growth due to GDD differences among years. The *RMSE* and *SE* in the mutual estimation were calculated for base-temperature increments of 1 °C, as shown in Fig. 3.3. The 2-year GDD integrated PLSR models were fitted, and the data from the other years were estimated. When the base temperature was 27 °C, the *RMSE* and *SE* values were at a minimum (0.66 g/m^2 and 0.62 g/m^2, respectively).

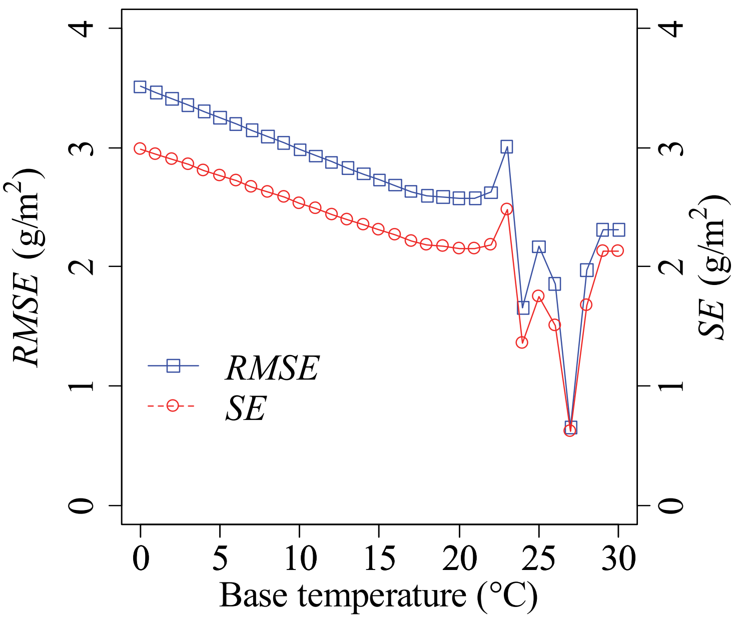

Fig. 3.3 *RMSE* and standard error (*SE*) in mutual estimation using 2-year GDD integrated models, as a function of base temperature

In the validation with the 2-year GDD integrated PLSR models, the *RMSE* and *RE* values ranged from 0.52 to 0.63 g/m^2 and 9.1 to 10%, respectively (Table 3.2). Thus, in terms of the accuracy of the internal validation, there were no significant differences between the GDD integrated and standard 1- and 2-year models. Table 3.2 also shows the results of mutual estimation using the 2-year GDD integrated PLSR models. When the 2010 data were estimated from the 2-year (2008 and 2009) GDD integrated PLSR model, the *RMSE* value decreased from 3.32 to 0.95 g/m^2. When the 2009 data were estimated from the 2-year (2008 and 2010) GDD integrated PLSR model, the *RMSE* value decreased from 1.29 to 0.50 g/m^2. Similarly, when the 2008 data were estimated from the 2-year (2009 and 2010) GDD integrated PLSR model, the *RMSE* value decreased from 1.82 to 0.55 g/m^2. Compared to the results of the 2-year PLSR model (Fig. 3.2, middle), the magnitude of the intercepts was clearly reduced (Fig. 3.2, right). Thus, temperature data are useful for establishing a model that is adaptable to the variance in growing conditions.

Further studies are required to investigate whether the GDD integrated PLSR model is useful for predicting the nitrogen content of other crops. It should also be determined whether the inclusion of other factors, such as daily range of temperature or radiation, may further improve the accuracy of the model. In this study ground-based remote sensing was used. Its spatial resolution is high and image acquisition can be done anytime except rainy weather unlike airborne or satellite remote sensing, although the area of application is small. The problem can be solved with the use of an unmanned aerial vehicle (UAV), such as Swain et al. (2010) used to estimate yield and biomass of a rice crop.

3.4 Conclusions

The extent to which the models overestimated and underestimated GDD variation and nitrogen content was examined to identify the most accurate model. It was inferred that hyperspectral imaging at 400 to 1000 nm could not predict variation in the amount of growth caused by weather variation expressed as GDD. Hence, the cumulative temperature data was included in the PLSR model, in which the 2-year GDD integrated PLSR model incorporated the reflectance and temperature data from 2 years. This study indicates that the combination of reflectance and temperature data could be used to construct a model that is adaptable to variance in growing conditions.

References

Bajwa, S., A. Mishra, and R. Norman. 2010. Canopy reflectance response to plant nitrogen accumulation in rice. *Precision Agriculture* 11(5):488-506.

Hansen, P., and J. Schjoerring. 2003. Reflectance measurement of canopy biomass and nitrogen status in wheat crops using normalized difference vegetation indices and partial least squares regression. *Remote sensing of Environment* 86(4):542-553.

Inamura, T. 2003. Correlation of the Amount of Nitrogen Accumulated in the Aboveground Biomass at Panicle Initiation and Nitrogen Content of Soil with the Nitrogen Uptake by Lowland Rice during the Period from Panicle Initiation to Heading. *Plant Production Science* 6(4):302-308.

McMaster, G. S., and W. Wilhelm. 1997. Growing degree-days: one equation, two interpretations. *Agricultural and Forest Meteorology* 87(4):291-300.

Nguyen, H. T., and B.-W. Lee. 2006. Assessment of rice leaf growth and nitrogen status by hyperspectral canopy reflectance and partial least square regression. *European Journal of Agronomy* 24(4):349-356.

Oppelt, N., and W. Mauser. 2004. Hyperspectral monitoring of physiological parameters of wheat during a vegetation period using AVIS data. *International Journal of Remote Sensing* 25(1):145-159.

Ozaki, K., T. Kobayashi, Y. Ohashi, and K. Kawase. 2012. Establishment of Predict Method to Regulate Desirable Spikelet Numbers and Protein Contents by Growth Diagnosis Production, and Application to 'Koshihikari' Cultivated in Tango Area, Kyoto Prefecture. *Bulletin of the Agriculture and Forestry Technology Department, Kyoto Prefectural Agriculture, Forestry and Fisheries Technology Center. Agriculture Section*(35):1-10.

Rouse Jr, J., R. Haas, J. Schell, and D. Deering. 1974. Monitoring vegetation systems in the Great Plains with ERTS. *NASA special publication* 351:309.

Ryu, C., M. Suguri, and M. Umeda. 2009. Model for predicting the nitrogen content of rice at panicle initiation stage using data from airborne hyperspectral remote sensing. *Biosystems engineering* 104(4):465-475.

Ryu, C., M. Suguri, and M. Umeda. 2011. Multivariate analysis of nitrogen content for rice at the heading stage using reflectance of airborne hyperspectral remote sensing. *Field Crops Research* 122(3):214-224.

Swain, K. C., S. J. Thomson, and H. P. Jayasuriya. 2010. Adoption of an unmanned helicopter for low-altitude remote sensing to estimate yield and total biomass of a rice crop. *Transactions of the ASABE* 53(1):21-27.

Tucker, C. J. 1979. Red and photographic infrared linear combinations for monitoring vegetation. *Remote sensing of Environment* 8(2):127-150.

Wang, F.-m., J.-f. Huang, and Z.-h. Lou. 2011. A comparison of three methods for estimating leaf area index of paddy rice from optimal hyperspectral bands. *Precision Agriculture* 12(3):439-447.

Went, F. 1953. The effect of temperature on plant growth. *Annual Review of Plant Physiology* 4(1):347-362.

Wold, S., M. Sjöström, and L. Eriksson. 2001. PLS-regression: a basic tool of chemometrics. *Chemometrics and intelligent laboratory systems* 58(2):109-130.

Xue, L., W. Cao, W. Luo, T. Dai, and Y. Zhu. 2004. Monitoring leaf nitrogen status in rice with canopy spectral reflectance. *Agronomy Journal* 96(1):135-142.

Chapter IV

Estimation of nitrogen content at heading stage

Abstract Ground-based hyperspectral imaging was used for estimating the nitrogen content of rice plants at heading stage. The images were separated into two parts: the rice plant and other elements using the equation of "*GNDVI–NDVI*". Ref_{RICE} was calculated as the ratio of the reflectance of the rice plant to that of a reference board. A partial least squares regression (PLSR) model that incorporated both the reflectance and growing degree-days (GDD) to account for differences in growing temperature conditions across a 3-year period. Three types of PLSR models were constructed: 1-year, 2-year, and 2-year GDD. Mutual estimation was used to infer the predictive power of the three models, which was calculated by estimating the values for the other years. The root mean square error of prediction (*RMSE*) of the mutual estimation for the 1-year and 2-year PLSR models was high because of overestimation and underestimation. In contrast, the *RMSE* of the mutual estimation for the 2-year GDD integrated PLSR models clearly decreased. This study indicates that the combination of reflectance and temperature data could be used to potentially construct an adaptable model to identify variance in growing conditions.

Keywords Ground-based hyperspectral imaging · Nitrogen content · Paddy rice · Heading stage · Growing degree-days · Growing degree-days integrated model

4.1 Introduction

Crop monitoring reduces the risk of poor control because it is critical for the estimation of crop growing status, quality and yield. The quality and quantity of rice grains are closely related to the growth and nitrogen content status at heading stage (Lee, 2002; Ntanos and Koutroubas, 2002). Thus, it is important to identify the growth and nitrogen content status of rice plants at heading stage. Moreover, it has also been confirmed that variable rate fertilizer application is adoptable for controlling the growth and nitrogen content status of rice plants uniformly. However, the accurate quantification of crop growth status by chemical analysis is destructive, laborious, and time-consuming.

Remote sensing has been investigated by many researchers and its ability to predict crop biochemical or physiological properties nondestructively using crop canopy reflectance has been demonstrated (Chen et al., 2013; Clevers and Kooistra, 2012; Nguyen and Lee, 2006; Oppelt and Mauser, 2004; Sims et al., 2013; Wang et al., 2008; Xue et al., 2004). Several remote sensing applications, such as satellite-based, aerial, and ground-based applications, have proven to be potential sources of reflectance data for the extraction of various spectral features and/or indices of vegetation (Ye et al., 2008). Hyperspectral sensor on the Earth Observing-1 was applied to map forest nutrient content (Sims et al., 2013). Several vegetation indices have been proposed for estimating canopy chlorophyll and nitrogen content using hyperspectral remote sensing (Clevers and Kooistra, 2012). In the case of rice plants, R_{830}/R_{550} ratio index (ratio of near-infrared to green reflectance) is effective for estimation of leaf nitrogen content (Inoue et al., 1998). R_{810}/R_{560} ratio index has also been developed to non-destructively monitor the nitrogen status of rice plants (Xue et al., 2004). Rice leaf nitrogen content can be estimated by high resolution measurements in the visible and near-infrared region (Inoue et al., 2000).

The spatial resolution of ground-based remote sensing is high and prediction capabilities may be improved, although the area of application is smaller than that of satellite-based or aerial methods. In ground-based remote sensing, spectrometers have been widely used, but the data obtained is one-dimensional. Consequently, the data includes the reflectance not only of the desired target but also of non-targets (White et al., 2000), such as soil background and ponding water in the case of rice paddies. A hyperspectral image, in contrast, provides a three-dimensional spatial and spectral data cube from which you can extract the reflectance of only the target. Partial least squares regression (PLSR) modeling has desirable properties that improve the precision of the modeling parameters with an increasing number of relevant variables and observations (Wold et al., 2001). PLSR analysis is one of the most efficient methods for extracting and creating reliable models in a wide range of fields (Nguyen and Lee, 2006) and when applied to hyperspectral reflectance data, it may be useful as an exploratory and predictive tool (Hansen and Schjoerring, 2003).

It can be difficult to estimate the nitrogen content of rice plants at heading stage using remote sensing techniques. Because leaf color obtained by remote sensing relates to not the amount of nitrogen but to the concentration of nitrogen. From a practical standpoint, an estimation model should have the ability to estimate crop status from new remote-sensing data with a certain level of precision or accuracy. Remote sensing models may be affected by differences in environmental variables, such as weather conditions (Ryu et al., 2009, 2011). Growing degree-day (GDD) is calculated from air temperature measurements and represents weather conditions that is frequently used to describe the timing of biological processes (McMaster and Wilhelm, 1997). Thus, we proposed a model based on a combination of both reflectance and GDD. To my knowledge, previous studies have not used hyperspectral imaging with a GDD to develop an estimation model of nitrogen content in rice at heading stage.

Therefore, this study aimed to construct a model that considered GDD over a 3-year period. The specific research objectives were (1) to establish a PLSR model to determine nitrogen content at heading stage using ground-based hyperspectral imaging, (2) to suggest an appropriate GDD-integrated model that worked across years, and (3) to compare the accuracy of conventional reflectance models and the suggested GDD-integrated model.

4.2 Materials and methods

4.2.1 Image processing

Images were analyzed using the Environment for Visualizing Images (ENVI) software (version 4.7; ITT Visual Information Solutions, Boulder, Colorado, USA) similar to what was done at the panicle initiation stage. See section 2.3.1 for details.

4.2.2 Rice plant sampling and chemical analysis

See section 2.4.2.

4.3 Results and Discussion

4.3.1 Measurement of vegetation data and canopy reflectance

Table 4.1 shows the measured nitrogen content at heading stage for three years. Due to strong wind during image acquisition, some images were defective and therefore were excluded from the analysis. Thus, the number of images was 24 in 2008, 29 in 2009, and 25 in 2010. Mean nitrogen content ranged from 6.92 to 12.68 g/m^2 in 2008, 8.14 to 9.80 g/m^2 in 2009, and 7.49 to 8.89 g/m^2 in 2010 among fields. The differences among years are significant ($P < 0.001$; ANOVA). Result of multiple comparison reveal presence of significant differences in the mean nitrogen content among years with a 1% level of significance.

Table 4.1 Summary for nitrogen content of rice plants at heading stage

Field	2008			2009			2010		
	n	Mean (g/m^2)	SD	*n*	Mean (g/m^2)	SD	*n*	Mean (g/m^2)	SD
1	5	6.92	0.69	8	8.21	1.27	6	8.05	0.84
2	6	11.93	1.58	8	9.37	1.29	6	8.19	0.99
3	6	12.68	1.71	5	9.80	1.87	5	8.89	1.81
4	7	9.58	1.80	8	8.14	1.09	8	7.49	0.40
Total	24	10.39	2.63	29	8.79	1.45	25	8.07	1.09

n: number of samples, SD: standard deviation

Figure 4.1 shows the mean reflectance of a rice plant (Ref_{RICE}) which was extracted by *GNDVI−NDVI*. The value of reflectance on the Y axis is over 1 due to the use of a gray color reference board. The reflectance of a rice plant is moderately variable in the visible region and variable in the NIR region. This result is in accordance with previous observations (Hansen and Schjoerring, 2003; Nguyen and Lee, 2006; Xue et al., 2004).

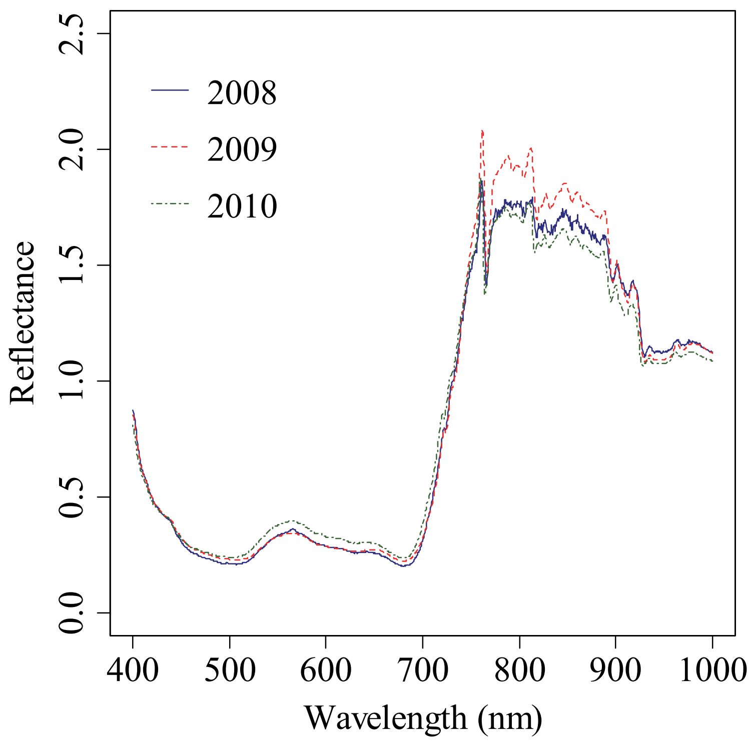

Fig. 4.1 Rice plant reflectance at heading stage

4.3.2 Performance of one-year PLSR model

The hyperspectral reflectance was related to the nitrogen content of rice plants at heading stage through PLSR analysis. Table 4.2 indicates that 1-year PLSR models may be considered to have good practical accuracy. The range in validation precision (R^2) from 0.45 to 0.84 may be due to differences among years in the variances of nitrogen content (Table 4.2). Compared to the calibration results, precision and accuracy (*RMSE* and *RE*) in validation are slightly lower, but these models may still be useful to predict the nitrogen content of rice plants at heading stage. Accordingly, the mutual predictions of each one-year PLSR model were calculated using the data in other years as the test set to determine the predictive potential of a model that considers growing condition. In mutual predictions with the 1-year PLSR models, *RMSE* ranged from 1.52 to 5.72 g/m^2 and *RE* ranged from 15.3 to 62.7% (Table 4.2). *RMSE* and *RE* for mutual prediction were much higher than those for validation. When 2008 1-year PLSR model and 2010 1-year PLSR model were used to estimate the remaining data, *RE* ranged from 18.8 to 32.9%. However, when 2008 and 2010 data are estimated with the 2009 1-year PLSR model, *RE* increased to 55.0% and 62.7%, respectively. Thus, a model that considers growing condition, the 2008 or 2010 1-year PLSR model might be better than the 2009 1-year PLSR model.

Figure 4.2, left shows the relationships between measured and estimated nitrogen content for the mutual estimation. When the 2008 1-year PLSR model is used to estimate the 2009 and 2010 data, the 2009 data were overestimated and the 2010 data were underestimated. With the 2009 1-year PLSR model, both 2008 and 2010 data were underestimated. Similarly, the 2010 1-year PLSR model prediction overestimated the 2009 data. It is desirable to narrow the distance between the over- and underestimation from mutual estimation. In model calibration, for the purpose of model adaptability, data collection is commonly conducted under varying nitrogen fertilization, irrigation, planting density, cultivar, and weather. Accordingly, a PLSR model based on two years' data (the 2-year PLSR model) was constructed to account for variation among years.

Table 4.2 Results of the calibration, leave-one-out cross validation, and mutual estimation analyses with the 1-year, 2-year, and 2-year GDD integrated PLSR models

Model type	Calibration						Validation			Mutual estimation			
	Data	*n*	LVs	R^2	*RMSE*	*RE*	R^2	*RMSE*	*RE*	Data	*n*	*RMSE*	*RE*
1-year reflectance	2008	24	2	0.88	0.88	8.5	0.84	1.03	9.9	2009	29	2.89	32.9
1-year reflectance	2008	24	2	0.88	0.88	8.5	0.84	1.03	9.9	2010	25	1.52	18.8
1-year reflectance	2009	29	3	0.78	0.67	7.6	0.61	0.89	10.1	2008	24	5.72	55.0
1-year reflectance	2009	29	3	0.78	0.67	7.6	0.61	0.89	10.1	2010	25	5.06	62.7
1-year reflectance	2010	25	3	0.65	0.63	7.8	0.45	0.80	9.9	2008	24	1.59	15.3
1-year reflectance	2010	25	3	0.65	0.63	7.8	0.45	0.80	9.9	2009	29	2.49	28.3
2-year reflectance	2008, 2009	53	3	0.71	1.17	12.3	0.65	1.29	13.5	2010	25	1.11	13.7
2-year reflectance	2008, 2010	49	4	0.91	0.69	7.5	0.84	0.90	9.7	2009	29	3.76	42.8
2-year reflectance	2009, 2010	54	4	0.74	0.67	7.9	0.61	0.83	9.8	2008	24	4.15	40.0
2-year reflectance + GDD	2008, 2009	53	3	0.78	1.02	10.7	0.74	1.12	11.8	2010	25	0.99	12.3
2-year reflectance + GDD	2008, 2010	49	4	0.88	0.78	8.5	0.83	0.93	10.1	2009	29	1.07	12.1
2-year reflectance + GDD	2009, 2010	54	4	0.73	0.69	8.2	0.59	0.85	10.1	2008	24	1.21	11.6

n: number of samples, LVs: number of latent variables, R^2: coefficient of determination, *RMSE*: root mean square error (g/m^2), *RE*: relative error (%)

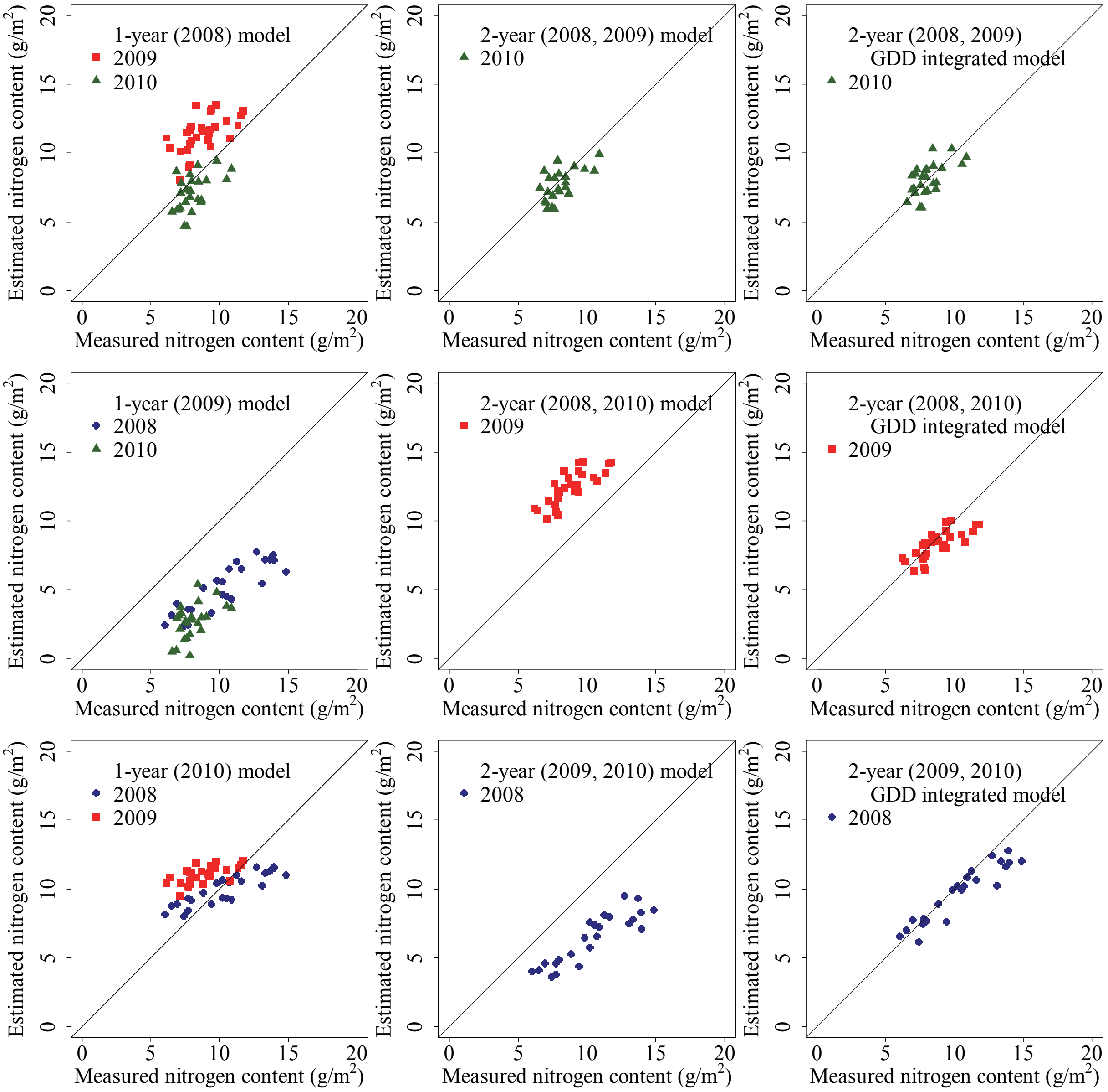

Fig. 4.2 Results of the mutual estimation with the 1-year (left), 2-year (middle), and 2-year GDD integrated (right) PLSR models

4.3.3 Performance of two-year PLSR model

Table 4.2 shows the results of PLSR analysis for nitrogen content using 2-year PLSR models. *RMSE* in validation ranges from 0.83 to 1.29 g/m^2 and *RE* range from 9.7 to 13.5%. This result indicates that there were no significant differences in accuracy between the 2- and 1-year PLSR models.

When the 2010 data was estimated by the 2-year PLSR model based on the 2008 and 2009 data, *RMSE* and *RE* were 1.11 g/m^2 and 13.7%, respectively. Thus, the accuracy is superior to that of mutual prediction with the 2008 or 2009 1-year PLSR models. While, when 2009 data was estimated by the 2-year PLSR model based on the remaining data, *RMSE* or *RE* is inferior to the result of mutual estimation with the 1-year PLSR models. Thus, when the model was constructed from data with big differences in weather conditions between years, the accuracy of 2-year model is lower than the 1-year PLSR models.

The relationships between estimated and measured values for the 2-year PLSR models are approximately parallel to the 1:1 line (Fig. 4.2 left and middle), suggesting that prediction ability might increase compared to the 1-year PLSR models. The 2-year PLSR model might thus be a potential model that considers growing condition. However, the intercept, or distance between the 1:1 line and an approximate fitted line through the estimated values, is nonzero (Fig. 4.2 left and middle).

4.3.4 Performance of the two-year GDD integrated model

Because all data tended to be overestimated or underestimated when nitrogen content was estimated by the 1-year PLSR models in mutual estimations, estimation accuracy was reduced (Table 4.2 and Fig. 4.2, left). The large and small values of GDD (Table 2.2 in Chapter II) follow this overestimation and underestimation. Specifically, 1-year PLSR models constructed under relatively high sum of GDD values tended to overestimate the relatively low sum of GDD data. In contrast, 1-year PLSR models constructed under relatively low sum of GDD values tend to underestimate relatively high summed GDD data. These observations indicate that temperature data could be used to correct the influence of GDD differences among years. Furthermore, these observations demonstrated that remote sensing using ground-based hyperspectral imaging from 400 to 1000 nm could not be used to explain the intercept, which is the distance from the 1:1 line to the slope of the estimated values. Therefore, the indirect influence of GDD on the growth rate could be quantified to improve the accuracy of the mutual estimation. Accordingly, the number of latent variables (LVs) for 2-year GDD integrated PLSR models was fixed at the number used for the 2-year PLSR models in order to quantify variation in the amount of growth due to weather variation. Incorporation of GDD data in the PLSR model required corresponding optimization.

GDD was calculated as the sum of average daily temperature subtracted from a base temperature in order to quantify the variation in the amount of growth due to weather differences among years.

RMSE and *SE* in the mutual prediction were calculated for base-temperature increments of 1 °C as shown in Fig. 4.3. The 2-year GDD integrated PLSR models were fitted and the remaining years' data were estimated. When the base temperature is 23°C or 27°C, *RMSE* and *SE* are at their minimum values (1.09 g/m^2 and 0.66 g/m^2, respectively). When the base temperature is 25°C, *RMSE* increases to 11 g/m^2. This is because the data in 2009 were estimated with high error (more than 18 g/m^2 in *RMSE*) by the 2008 and 2010 2-year GDD integrated PLSR model due to the big differences in weather conditions between 2009 and the remaining years. Table 4.2 shows the result of 2-year GDD integrated PLSR model calibration and validation. In validation, R^2 and *RMSE* range from 0.59 to 0.83 and 0.85 to 1.12 g/m^2, respectively, while *RE* was approximately 11%. Thus, in terms of precision and accuracy in internal validation, there were no significant differences between the 2-year GDD integrated PLSR model and the 2-year PLSR models.

Table 4.2 shows the result of mutual estimation using the 2-year GDD integrated PLSR models. When the 2010 data was estimated with the 2-year (2008 and 2009) GDD integrated PLSR model, *RMSE* and *RE* decreased to 0.99 g/m^2 and 12.3%, respectively. When the 2009 data was predicted by the 2-year (2008 and 2010) GDD integrated PLSR model, *RMSE* and *RE* decreased to 1.07 g/m^2 and 12.1%, respectively. Similarly, when the 2008 data were estimated by the 2-year (2009 and 2010) GDD integrated PLSR model, *RMSE* and *RE* decreased to 1.21 g/m^2 and 11.6%, respectively. Differences of the environmental factor such as weather conditions may not be considered by a PLSR model derived from only hyperspectral data because in the result of mutual estimation, bias is nonzero as shown in Fig. 4.2, left and middle. In the areas of crop phenology and development, the concept of heat units, expressed in GDD, is used to describe phenological events (McMaster and Wilhelm, 1997). Therefore by incorporating optimized GDD, the accuracy of the 2-year GDD integrated PLSR models may be higher than that of the 2-year PLSR models.

Figure 4.2, right shows the result of mutual estimation with the 2-year GDD integrated PLSR models. Compared with the result of the 2-year PLSR model shown in Fig. 4.2, middle, the intercepts are clearly reduced in magnitude. *RMSE* was decreased by 2.94 g/m^2 in 2008, 2.69 g/m^2 in 2009 and 0.02 g/m^2 in 2010. It means that the temperature data are useful for establishment of a model considered growing condition.

Further studies should investigate whether the GDD integrated PLSR model can be applied to other crops. It should also be determined whether the additional factors such as daily range of temperature or radiation can improve the model accuracy.

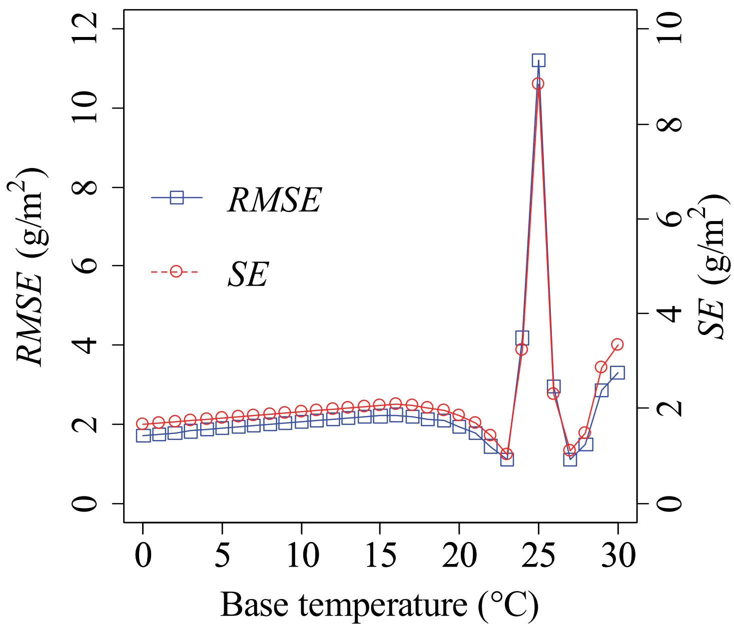

Fig. 4.3 *RMSE* and standard error (*SE*) in mutual estimation using 2-year GDD integrated PLSR models as a function of base temperature

4.4 Conclusions

Examination aimed at discovering a more accurate estimation model suggested a correspondence between GDD variation and nitrogen content over- and underestimation. It was inferred that hyperspectral imaging at 400 to 1000 nm could not estimate variation in the amount of growth caused by weather variation expressed as GDD. Accordingly, the cumulative temperature data was included in the PLSR model, leading to a model (GDD integrated model) incorporating two years' reflectance and temperature data. The combined reflectance and temperature data were useful for constructing a model considered growing condition.

References

Chen, P., J. Wang, W. Huang, N. Tremblay, and Y. Ou. 2013. Critical Nitrogen Curve and Remote Detection of Nitrogen Nutrition Index for Corn in the Northwestern Plain of Shandong Province, China. *IEEE journal of selected topics in applied earth observations and remote sensing* 6(2):682-689.

Clevers, J. G. P. W., and L. Kooistra. 2012. Using Hyperspectral Remote Sensing Data for Retrieving Canopy Chlorophyll and Nitrogen Content. *IEEE journal of selected topics in applied earth observations and remote sensing* 5(2):574-583.

Evri, M., T. Akiyama, and K. Kawamura. 2008. Spectrum analysis of hyperspectral red edge position to predict rice biophysical parameters and grain weight. *Japan Society of Photogrammetry and Remote Sensing* 47(2):4-15.

Hansen, P., and J. Schjoerring. 2003. Reflectance measurement of canopy biomass and nitrogen status in wheat crops using normalized difference vegetation indices and partial least squares regression. *Remote sensing of Environment* 86(4):542-553.

Inoue, Y., M. S. Moran, and T. Horie. 1998. Analysis of spectral measurements in paddy field for predicting rice growth and yield based on a simple crop simulation model. *Plant Production Science* 1:269-279.

Inoue, Y., J. Qi, Y. Nouvellon, and M. Moran. 2000. Hyperspectral and directional remote sensing measurements of rice canopies for estimation of plant growth variables. In *Geoscience and Remote Sensing Symposium, 2000. Proceedings. IGARSS 2000. IEEE 2000 International*. IEEE.

Lee, B.-W. 2002. Spikelet number estimation model using nitrogen nutrition status and biomass at panicle initiation and heading stage of rice. *Korean Journal of Crop Science* 47(5):390-394.

McMaster, G. S., and W. Wilhelm. 1997. Growing degree-days: one equation, two interpretations. *Agricultural and Forest Meteorology* 87(4):291-300.

Nguyen, H. T., and B.-W. Lee. 2006. Assessment of rice leaf growth and nitrogen status by hyperspectral canopy reflectance and partial least square regression. *European Journal of Agronomy* 24(4):349-356.

Ntanos, D., and S. Koutroubas. 2002. Dry matter and N accumulation and translocation for Indica and Japonica rice under Mediterranean conditions. *Field Crops Research* 74(1):93-101.

Oppelt, N., and W. Mauser. 2004. Hyperspectral monitoring of physiological parameters of wheat during a vegetation period using AVIS data. *International Journal of Remote Sensing*

25(1):145-159.

Ryu, C., M. Suguri, and M. Umeda. 2009. Model for predicting the nitrogen content of rice at panicle initiation stage using data from airborne hyperspectral remote sensing. *Biosystems engineering* 104(4):465-475.

Ryu, C., M. Suguri, and M. Umeda. 2011. Multivariate analysis of nitrogen content for rice at the heading stage using reflectance of airborne hyperspectral remote sensing. *Field Crops Research* 122(3):214-224.

Sims, N. C., D. Culvenor, G. Newnham, N. C. Coops, and P. Hopmans. 2013. Towards the Operational Use of Satellite Hyperspectral Image Data for Mapping Nutrient Status and Fertilizer Requirements in Australian Plantation Forests. *IEEE journal of selected topics in applied earth observations and remote sensing* 6(2):320-328.

Wang, F. M., J. F. Huang, and X. Z. Wang. 2008. Identification of optimal hyperspectral bands for estimation of rice biophysical parameters. *Journal of integrative plant biology* 50(3):291-299.

Went, F. 1953. The effect of temperature on plant growth. *Annual Review of Plant Physiology* 4(1):347-362.

White, J., C. Trotter, L. Brown, and N. Scott. 2000. Nitrogen concentration in New Zealand vegetation foliage derived from laboratory and field spectrometry. *International Journal of Remote Sensing* 21(12):2525-2531.

Wold, S., M. Sjöström, and L. Eriksson. 2001. PLS-regression: a basic tool of chemometrics. *Chemometrics and intelligent laboratory systems* 58(2):109-130.

Xue, L., W. Cao, W. Luo, T. Dai, and Y. Zhu. 2004. Monitoring leaf nitrogen status in rice with canopy spectral reflectance. *Agronomy Journal* 96(1):135-142.

Ye, X., K. Sakai, H. Okamoto, and L. O. Garciano. 2008. A ground-based hyperspectral imaging system for characterizing vegetation spectral features. *Computers and electronics in Agriculture* 63(1):13-21.

Chapter V

Estimation of rice protein content just before harvest

Abstract Protein content, which a representative index of rice taste quality, must be estimated in order to plan harvesting, as well as next year's basal dressing fertilizer application. Ground-based hyperspectral imaging with high resolution (1 × 1 mm per pixel) was used for estimating the protein content of brown rice just before harvest. This chapter compares the estimation accuracy of rice protein content estimation models generated from the mean reflectances of five regions of interest (ROIs): the overall target area, non-canopy area (stems and soil), canopy area (leaves, yellow leaves, and ears), leaf area, and ear and yellow leaf area. The size of the targeted sampling area was 85 × 85 cm. An $R+G+B$ histogram and a $GNDVI-NDVI$ image were used to separate the targeted area into the individual ROIs. The values of the coefficient of determination R^2 and the root mean square error of prediction ($RMSE$) were similar for each model: R^2 ranged from 0.83 to 0.86 and $RMSE$ ranged from 0.27% to 0.30% for all models except for the non-canopy model, where R^2 = 0.76 and $RMSE$ = 0.35%. There were no significant differences in the magnitude of the estimation error among all models according to an analysis of variance (ANOVA). These results indicate that it is not necessary to obtain an unmanned aerial vehicle (UAV) image with a ground resolution that is greater than 85 × 85 cm per pixel to estimate rice protein content before harvest. This result should provide useful information for deciding the altitude of UAVs for imaging rice fields.

Keywords Ground-based hyperspectral imaging · Protein content · Paddy rice · Harvest · Region of interest

5.1 Introduction

Recently, farmers in northeast Asia (the northern part of China, Japan, Korea, and Taiwan) have focused on not only grain yield but also grain quality. Merchants also pay close attention to grain quality. For instance, some Japanese agricultural cooperatives sell rice at a price that reflects the taste quality of the rice as measured by a rice taste analyzer. There are three main chemical components that contribute to rice taste quality: protein, amylose, and fatty acid content. These factors negatively affect quality. Fatty acid is affected by the length of storage (Ryu et al., 2011a). Amylose content is mainly affected by the rice variety and growing temperature during maturation (Asaka and Shiga, 2003). This means that fatty acid and amylose were not controllable. While, protein content is affected by the amount of top-dressing (Ozaki et al., 2012). Therefore, the control of the protein content is a key factor for field management, and it is important to assess the distribution of rice protein content in order to adaptively apply next year's fertilizer. Generally, protein content differs within, as well as among, rice fields. However, it is difficult to measure the protein content distribution to this degree of accuracy. If the estimation of protein content in rice before harvest is possible, the harvest and storage of rice depending on its taste quality is also possible. Moreover, if field management data such as the basal dressing and top-dressing applications, as well as the distribution of the protein content just before harvest are inputted into a geographic information system (GIS), the control of rice taste quality and yield may be possible.

Remote sensing has been widely used in agriculture, as its ability to non-destructively predict crop biochemical properties has been proven. There are several types of remote sensing systems. Satellite or airborne remote sensing systems that can be used for large areas. However, acquiring this image data is usually quite expensive and the spatial resolution is generally low (Ye et al., 2008). In addition, clear images can seldom be obtained during the cropping period in Japan because of its location in a monsoon zone (Ishiguro et al., 1993). The relationship between canopy reflectance and rice protein content has been previously studied by Ryu et al. (2011a) and Asaka and Shiga (2003). The former applied the green normalized difference vegetation index (*GNDVI*) to airborne imaging data and the latter applied the normalized difference vegetation index (*NDVI*) to images obtained by satellite to estimate the rice protein content. In contrast, with ground-based remote sensing, the spatial resolution is high and images acquisition can be done anytime except during rainy weather, although the area that can be imaged is smaller. However, the use of unmanned aerial vehicles (UAVs) as a platform for remote sensing is now commonplace (Honkavaara et al., 2013; Turner et al., 2014; Uto et al., 2013) and the difficulty of imaging large fields is thus resolved. Spectroradiometers have been widely used for ground-based remote sensing, although the data obtained is one-dimensional. As a result, the data includes not only the reflectance of the desired target, but also that of non-targets, such as soil background. By contrast, a hyperspectral camera provides three-dimensional images that includes spectral information for each pixel. However, in the case of such close-range imaging systems, preprocessing is needed to obtain true plant spectral information because of the various illumination levels on the leaf surface (Uto and Kosugi, 2013a, b; Vigneau et al., 2011). When appropriate preprocessing is applied to a hyperspectral image, the accuracy of an estimation model is often enhanced.

The canopy structure of rice plants before harvest is composed of ears and leaves. Ishii and Katano (2008) estimated the rice protein content from the leaf blade's SPAD-502 chlorophyll meter (Konica Minolta, Inc., Tokyo, Japan) value. Onoyama et al. (2011) estimated it from the reflectance of rough rice. Ryu et al. (2011a) estimated it from the whole canopy reflectance of the rice plant. However, the exact part of the rice plant that is suitable for the estimation of the rice protein content has not yet been identified. Thus, I applied region of interest (ROI) analysis, which segments the image into categories such as the leaf, ear, or whole rice plant, extract the spectral information of each segment, and then compare the model accuracies derived from each ROI reflectance. From this information, the appropriate preprocessing can be proposed for the estimation of protein content of rice just before harvest. Therefore, the aim of this study is to establish estimation models generated from the reflectance of various ROIs and compare their accuracies.

5.2 Materials and methods

5.2.1 Image processing for segmenting five regions of interest (ROIs)

The acquired images were processed using mouse-based software written in Java. See section 2.3.2 for details.

5.2.2 Rice plant sampling and measurement of protein content

The protein content of the brown rice was measured using a rice grain taste analyzer. See section 2.4.3 for details.

5.3 Results and Discussion

5.3.1 Measurement of protein content of brown rice

Table 5.1 shows the protein content, measured on a dry basis, of brown rice just before harvesting for three years. Because of strong winds during image acquisition, two images in 2008 were unusable and therefore were excluded from the analysis. The mean values and standard deviations of the protein content were 7.0% and 0.5% in 2008, 7.9% and 0.4% in 2009, and 8.3%

and 0.5% in 2010. There were significant differences in the mean values of the protein content over the three years with a 0.1% level of significance (ANOVA). The results of Tukey's multiple comparisons show that there were significant differences in the mean values of the protein content between 2008 and both other years with a 0.1% level of significance, and there were significant differences in the mean values of protein content between 2009 and 2010 with a 1% level of significance. The distribution of protein content data collected for this study is comparable to the distribution of rice protein content in Japan. The protein content of rice is influenced by the amount of nitrogen fertilizer used as topdressing (Ryu et al., 2005), temperature during ripening (Matsue, 1995), water management (Cheng et al., 2003), and harvest timing (Matsue et al., 1991).

Table 5.1 Summary of the protein content of brown rice

Field	2008			2009			2010		
	n	Mean (%)	SD	*n*	Mean (%)	SD	*n*	Mean (%)	SD
1	10	6.5	0.2	8	7.7	0.3	8	8.6	0.4
2	8	7.5	0.3	8	8.0	0.4	8	8.1	0.7
3	6	7.1	0.2	8	8.3	0.4	8	8.5	0.4
4	8	6.8	0.2	9	7.9	0.3	8	8.0	0.3
Total	32	7.0	0.5	33	7.9	0.4	32	8.3	0.5

n: number of samples, SD: standard deviation

5.3.2 Reflectance of five ROIs

I applied the proposed image processing algorithm to the hyperspectral images of rice plants before harvest. Example ROIs for each condition, as described in Table 2.4 (Section 2.3.2), are shown in white in Fig. 5.1. ROI-I was segmented using mouse-based software. Figure 5.1(d) demonstrates that the algorithm is able to determine the canopy area. In all images, the $R+G+B$ histogram method (Section 2.3.2) successfully separated the canopy and non-canopy areas. In the canopy area, the leaves and ears were separated using the $GNDVI-NDVI$ histogram, where leaves were black and ears were lighter colors in the $GNDVI-NDVI$ image (Fig. 2.8, c). Figure 5.2 shows the raw spectra of ear, leaf, and yellow leaf. As can be seen from Fig. 5.2, $GNDVI > NDVI$ for ear pixels and $GNDVI < NDVI$ for leaf pixels because the reflectance intensity at the red edge varies greatly between them. Therefore, the threshold value of $GNDVI-NDVI$ was set to zero. Figure 5.2 also shows that it is difficult to distinguish between ear pixels and yellow leaf pixels because of the similarity of their spectra. Thus, ROI-V includes not only ear pixels, but also yellow leaf pixels. However, this does not cause a problem in establishing the PLSR model because of their spectral similarities. When judging the ROIs by human eye, the proposed processing algorithm successfully extracts the desired regions.

Figure 5.3 shows the mean reflectance at each of the ROIs ($R_{Corrected\_ROI}$). The value of reflectance on the y-axis is greater than one because of the use of the gray color reference board. In general, the reflectance increases in the green region, decreases at the red edge, and is higher in the NIR region than the other regions. The reflectance of each ROI seems to be in accordance with the general features of plant reflectance, although the characteristics of ROI-II are small because of the low illumination level. ROI-V, which comprises the regions of ear and yellow leaf, shows a high reflectance at the red edge compared with the others because of the low content ratio of chlorophyll.

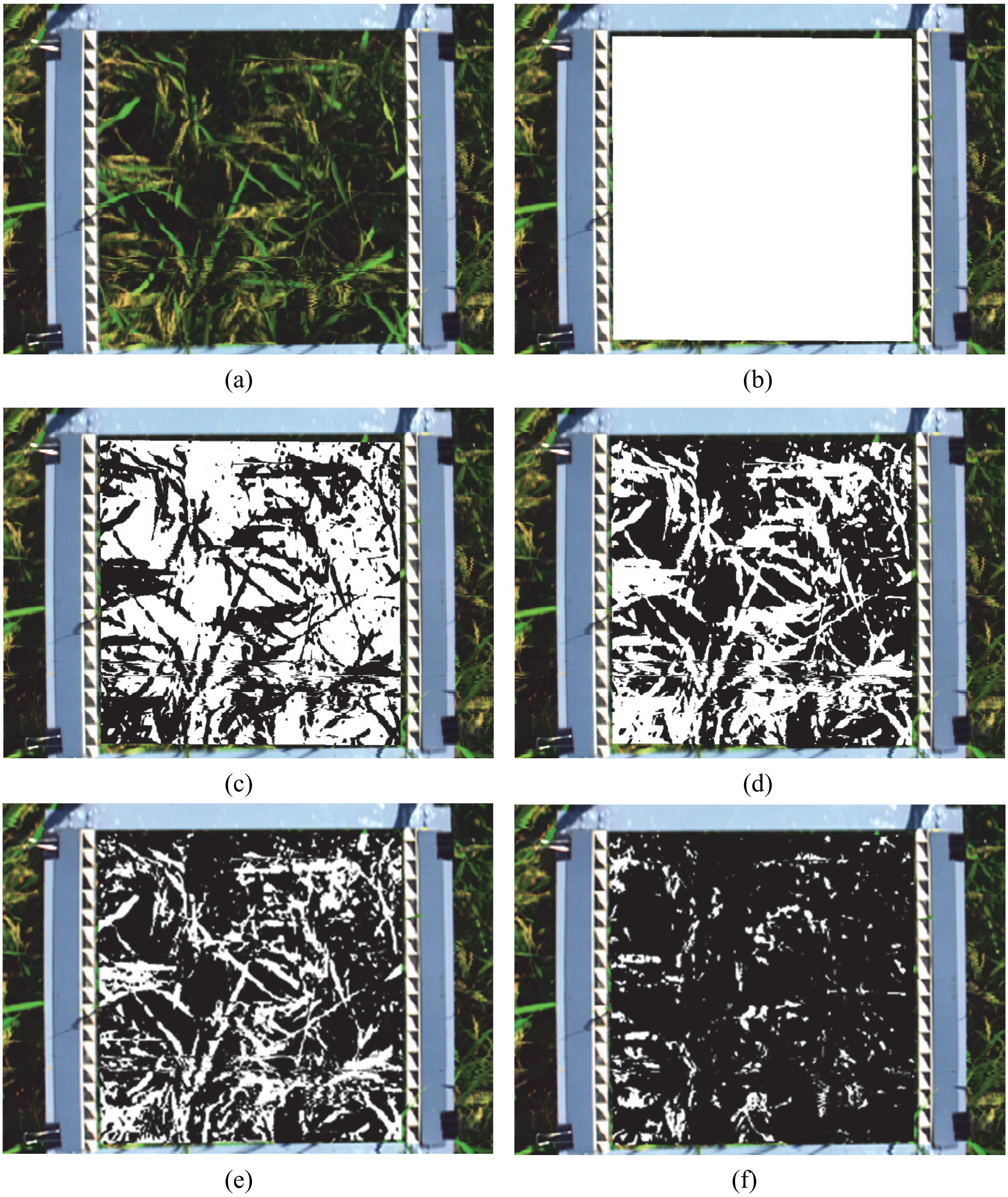

Fig. 5.1 ROI images: (a) RGB image, (b) ROI-I: target area, (c) ROI-II: non-canopy area, (d) ROI-III: canopy area, (e) ROI-IV: leaf area, and (f) ROI-V: ear area

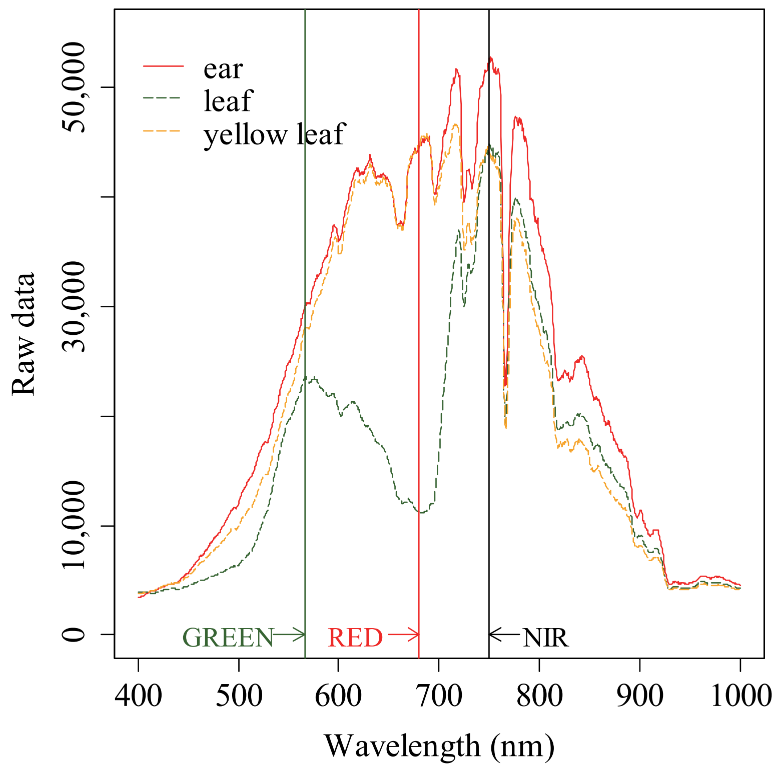

Fig. 5.2 Raw spectral of ear, leaf and yellow leaf

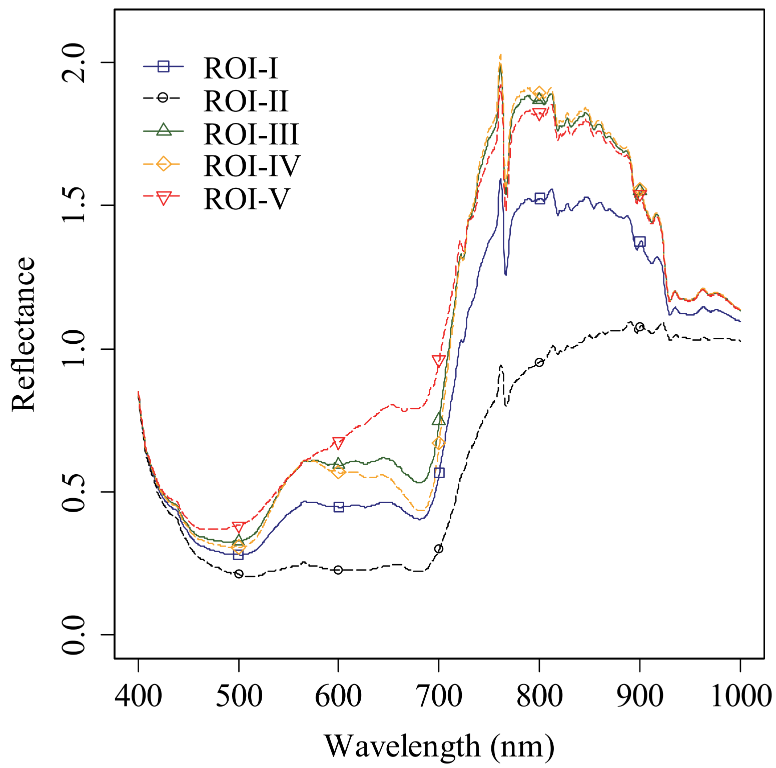

Fig. 5.3 Mean spectral reflectance of five ROIs

5.3.3 Partial least squares regression (PLSR) models generated from five ROIs

In this study, hyperspectral, high-resolution images were used for ROI analysis. The size of the target sampling area was 85 × 85 cm and the spatial resolution of the images was approximately 1 × 1 mm per pixel. The hyperspectral reflectances of all ROIs were related to the protein content of the rice plants just before harvest according to PLSR analysis. The accuracy of the five PLSR models using leave-one-out cross-validation was determined and assessed, and Table 5.2 shows the results. In this table, the reflectance of all ROIs led to high R^2 (> 0.76) with low *RMSE* (< 0.35%) in the validation results. All values of R^2 were similar (ranging from 0.83 to 0.86), except for that of the ROI-II model (R^2 = 0.76). The best result occurred when the reflectance of the leaf pixels (ROI-IV) was used for the estimation model: R^2 and *RMSE* were 0.86 and 0.27%, respectively. On the other hand, the worst result occurred when the reflectance of the non-canopy or shadowed pixels (ROI-II) was used for the estimation model: R^2 and *RMSE* were 0.76 and 0.35%, respectively. This is because the shadowed ROI-II was corrected using the well-illuminated reference board. Thus, the illumination level was not properly corrected in the ROI-II model. However, no significant differences in the magnitude of the estimated error among all ROI PLSR models as a result of ANOVA were observed. This indicates that the mixed pixel model (ROI-I), consisting of the pixels of the leaves, stems, ears (including yellow leaves), and their shadowed pixels is not different from the models constructed with the individual parts in terms of model accuracy, although the reflectance differs among them (Fig. 5.3). This result is convenient for UAV hyperspectral remote sensing (on the order of centimeters) or airborne hyperspectral remote sensing (on the order of several to tens of centimeters) because the mixed pixels do not affect model accuracy in the case of rice protein content estimation. From the point of view of saving processing time, not segmenting the image (i.e., using ROI-I) is recommended.

Table 5.2 Results of the PLSR models calibration and leave-one-out cross-validation generated from five ROIs

ROI	*n*	LVs	Calibration			Validation		
			R^2	*RMSE*	*RE*	R^2	*RMSE*	*RE*
I	97	13	0.94	0.17	2.2	0.83	0.29	3.8
II	97	11	0.90	0.22	2.9	0.76	0.35	4.6
III	97	12	0.94	0.18	2.4	0.83	0.30	3.8
IV	97	16	0.97	0.13	1.7	0.86	0.27	3.4
V	97	12	0.93	0.19	2.4	0.83	0.30	3.9

n: number of samples, LVs: number of latent variables, R^2: coefficient of determination, *RMSE*: root mean square error (%), *RE*: relative error (%)

5.4 Conclusions

In this study, ground-based hyperspectral and high resolution images were used to compare the accuracy of the proposed segmentation algorithm to estimate rice protein content just before harvest. The reflectance of all ROIs led to high R^2 (> 0.76) with low *RMSE* (< 0.35%). Thus, protein content of brown rice before harvest can be estimated using ground-based hyperspectral imaging. As a result of the ROI analysis, no significant differences in the accuracies of the estimation models were found. Therefore, I conclude that it is not necessary to obtain a UAV image with a ground resolution that is greater than 85 × 85 cm per pixel to estimate rice protein content just before harvest. However, further studies should investigate whether other stages of rice plant growth, such as the heading stage or other crops provide the same result. These investigations could provide useful information for planning the altitude of imaging platforms such as UAVs.

References

Asaka, D., and H. Shiga. 2003. Estimating rice grain protein contents with SPOT/HRV data acquired at maturing stage. *Journal of the Remote Sensing Society of Japan* 23(5):451-457.

Cheng, W., G. Zhang, G. Zhao, H. Yao, and H. Xu. 2003. Variation in rice quality of different cultivars and grain positions as affected by water management. *Field Crops Research* 80(3):245-252.

Honkavaara, E., H. Saari, J. Kaivosoja, I. Polonen, T. Hakala, P. Litkey, J. Makynen, and L. Pesonen. 2013. Processing and Assessment of Spectrometric, Stereoscopic Imagery Collected Using a Lightweight UAV Spectral Camera for Precision Agriculture. *Remote Sensing* 5(10):5006-5039.

Ishiguro, E., M. K. Kumar, Y. Hidaka, S. Yoshida, M. Sato, M. Miyazato, and J. Y. Chen. 1993. Use of rice response characteristics in area estimation by LANDSAT/TM and MOS-1 satellites data. *ISPRS journal of photogrammetry and remote sensing* 48(1):26-32.

Matsue, Y. 1995. Studies on Palatability of Rice in Northern Kyushu. V. Influence of abnormal weather in 1993 on the palatability and physicochemical characteristics of rice. *The Crop Science Society of Japan* 64(4):709-713.

Matsue, Y., K. Mizuta, K. Furuno, and T. Yoshida. 1991. Studies on Palatability of Rice Grown in Northern Kyushu. II. Effects of harvest time on palatability and physicochemical properties of milled rice. *Japanese Journal of Crop Science* 60(4):497-503.

Onoyama, H., C. Ryu, M. Suguri, and M. Iida. 2011. Estimation of Rice Protein Content Using Ground-Based Hyperspectral Remote Sensing. *Engineering in Agriculture, Environment and Food* 4(3):71-76.

Ozaki, K., T. Kobayashi, Y. Ohashi, and K. Kawase. 2012. Establishment of Predict Method to Regulate Desirable Spikelet Numbers and Protein Contents by Growth Diagnosis Production, and Application to 'Koshihikari' Cultivated in Tango Area, Kyoto Prefecture. *Bulletin of the Agriculture and Forestry Technology Department, Kyoto Prefectural Agriculture, Forestry and Fisheries Technology Center. Agriculture Section*(35):1-10.

Ryu, C., M. Iida, Y. Nishiike, and M. Umeda. 2005. Influence of several doses of nitrogen fertilizer on rice taste and grain yield. *Journal of the Japanese Society of Agricultural Machinery*.

Ryu, C., M. Suguri, M. Iida, M. Umeda, and C. Lee. 2011. Integrating remote sensing and GIS for prediction of rice protein contents. *Precision Agriculture* 12(3):378-394.

Turner, D., A. Lucieer, Z. Malenovsky, D. H. King, and S. A. Robinson. 2014. Spatial Co-

Registration of Ultra-High Resolution Visible, Multispectral and Thermal Images Acquired with a Micro-UAV over Antarctic Moss Beds. *Remote Sensing* 6(5):4003-4024.

Uto, K., and Y. Kosugi. 2013a. Estimation of Lambert parameter based on leaf-scale hyperspectral images using dichromatic model-based PCA. *International Journal of Remote Sensing* 34(4):1386-1412.

Uto, K., and Y. Kosugi. 2013b. Leaf parameter estimation based on leaf scale hyperspectral imagery. *IEEE J. Sel. Top. Appl. Earth Obs. Remote Sens* 6:699-707.

Uto, K., H. Seki, G. Saito, and Y. Kosugi. 2013. Characterization of Rice Paddies by a UAV-Mounted Miniature Hyperspectral Sensor System. *IEEE journal of selected topics in applied earth observations and remote sensing* 6(2):851-860.

Vigneau, N., M. Ecarnot, G. Rabatel, and P. Roumet. 2011. Potential of field hyperspectral imaging as a non destructive method to assess leaf nitrogen content in Wheat. *Field Crops Research* 122(1):25-31.

Ye, X., K. Sakai, H. Okamoto, and L. O. Garciano. 2008. A ground-based hyperspectral imaging system for characterizing vegetation spectral features. *Computers and electronics in Agriculture* 63(1):13-21.

Chapter VI

Conclusions and Future Research

6.1 Conclusions

In this study, ground-based hyperspectral imaging with high resolution (1 × 1 mm per pixel) was applied to rice plants at panicle initiation stage, at heading stage and just before harvest in order to estimate the nitrogen content of rice plants and protein content of brown rice.

1. It was demonstrated that a partial least squares regression (PLSR) model that incorporates both the reflectance and growing degree-days (GDD) is sufficiently adaptable to variance in interannual growing conditions to predict the nitrogen content of rice at panicle initiation stage. It was shown that that hyperspectral imaging at 400 to 1000 nm could not predict variation in the amount of growth caused by weather variation expressed as GDD; hence, cumulative temperature data was included in the GDD integrated PLSR model. It was confirmed that the greater accuracy of the GDD integrated model by comparing it against 1- and 2-year models that did not incorporate GDD, both of which exhibited major overestimation and underestimation of the actual datasets. Hence, a combination of reflectance and temperature data could potentially be used to construct adaptable models that identify variance in the growing conditions for different growth-stages of rice or other agricultural crops, which would help improve crop management decision and reduced economic costs by applying appropriate quantities of fertilizer.

2. It was also demonstrated that a PLSR model that incorporates both the reflectance and GDD is sufficiently adaptable to variance in interannual growing conditions to predict the nitrogen content of rice at heading stage.

3. The estimation accuracy of rice protein content estimation models generated from the mean reflectances of five regions of interest (ROIs): the overall target area, non-canopy area (stems and soil), canopy area (leaves, yellow leaves, and ears), leaf area, and ear and yellow leaf area were compared. There were no significant differences in the magnitude of the

estimation error among all models according to an analysis of variance (ANOVA) and all models could estimate rice protein content with high accuracy. These results indicate that high resolution images are not needed for the estimation of rice protein content before harvest. These results also could provide useful information for planning the altitude of imaging platforms such as UAVs.

6.2 Future Research

This thesis presents ground-based hyperspectral imaging system of rice plants. The GDD integrated model shows sufficiently predictive power against the growth of rice plants at panicle initiation stage and at heading stage. The PLSR model using hyperspectral canopy reflectance has high estimation precision of protein content just before harvest. However, there are further areas and gaps that needed to be explored.

1. In section 2.3.1, images were analyzed using the ENVI software and the threshold values to separate the rice plant and the other elements were manually selected. To reduce tedious manual image processing and to process images on a fixed criterion, an application of pattern recognition and machine learning will be needed.

2. In chapter III and IV, GDD was used to express the amount of growth caused by growing temperature variation among years. More direct expression to estimate the number of leaves are needed for estimating the amount of rice plants` nitrogen content. It could be expressed as a function of available nitrogen content and the ground temperature.
   There might be other reasons why the overestimation and underestimation were exhibited. One is the multiple reflection because of the differences in weather conditions among years, and the other is red edge shift. The former means that the increase of the number of leaves would affect the degree of multiple reflection, thereby affecting the reflected light level. The latter would affect in establishing PLSR model. The red edge position move to longer wavelengths until close to heading stage and otherwise shifted to shorter wavelengths after heading stage (Evri et al., 2008). Previous studies have identified the important spectral bands that are related to the crop vegetation using PLSR analysis and stepwise multiple linear regression using hyperspectral remote sensing and they have revealed that the red

edge is one of the critical bands for estimation of crop vegetation (Hansen and Schjoerring, 2003; Nguyen and Lee, 2006; Ryu et al., 2009). In the case of hyperspectral remote sensing, the effect of the red edge shift might have a significant impact on estimation modeling.

3. The spatial resolution of ground-based remote sensing is high and image acquisition is possible anytime except during rainy weather, unlike airborne-based or satellite-based image acquisition. However, the area of application is small. Thus, UAV-based remote sensing will need to be studied. UAV-based hyperspectral imagery could be pursued in the future.

References

Evri, M., T. Akiyama, and K. Kawamura. 2008. Spectrum analysis of hyperspectral red edge position to predict rice biophysical parameters and grain weight. *Japan Society of Photogrammetry and Remote Sensing* 47(2):4-15.

Hansen, P., and J. Schjoerring. 2003. Reflectance measurement of canopy biomass and nitrogen status in wheat crops using normalized difference vegetation indices and partial least squares regression. *Remote sensing of Environment* 86(4):542-553.

Nguyen, H. T., and B.-W. Lee. 2006. Assessment of rice leaf growth and nitrogen status by hyperspectral canopy reflectance and partial least square regression. *European Journal of Agronomy* 24(4):349-356.

Ryu, C., M. Suguri, and M. Umeda. 2009. Model for predicting the nitrogen content of rice at panicle initiation stage using data from airborne hyperspectral remote sensing. *Biosystems engineering* 104(4):465-475.